BBA - Molecular Basis of Disease 1870 (2024) 166980

Contents lists available at ScienceDirect

BBA - Molecular Basis of Disease

journal homepage: www.elsevier.com/locate/bbadis

NPC1-like phenotype, with intracellular cholesterol accumulation and altered mTORC1 signaling in models of Parkinson's disease

Inês Caria [a], Maria João Nunes [a,b], Viviana Ciraci [a], Andreia Neves Carvalho [a,b], Catarina Ranito [a], Susana G. Santos [a], Maria João Gama [a,b], Margarida Castro-Caldas [a,c], Cecília M.P. Rodrigues [a,b], Jorge L. Ruas [b,d], Elsa Rodrigues [a,b,*]

[a] Research Institute for Medicines (iMed.ULisboa), Faculty of Pharmacy, Universidade de Lisboa, Portugal
[b] Department of Pharmaceutical Sciences and Medicines, Faculty of Pharmacy, Universidade de Lisboa, Portugal
[c] UCIBIO, Department of Life Sciences, NOVA School of Science and Technology, Universidade NOVA de Lisboa, Caparica, Portugal
[d] Department of Physiology and Pharmacology, Karolinska Institutet, Stockholm, Sweden

ARTICLE INFO

Keywords:
Brain cholesterol metabolism
Mitochondria dysfunction
Lysosomes
NPC1
Parkinson's disease

ABSTRACT

Disruption of brain cholesterol homeostasis has been implicated in neurodegeneration. Nevertheless, the role of cholesterol in Parkinson's Disease (PD) remains unclear. We have used N2a mouse neuroblastoma cells and primary cultures of mouse neurons and 1-methyl-4-phenylpyridinium (MPP^+), a known mitochondrial complex I inhibitor and the toxic metabolite of 1-methyl-4-phenyl-1,2,3,6-tetrahydropyridine (MPTP), known to trigger a cascade of events associated with PD neuropathological features. Simultaneously, we utilized other mitochondrial toxins, including antimycin A, oligomycin, and carbonyl cyanide chlorophenylhydrazone. MPP^+ treatment resulted in elevated levels of total cholesterol and in a Niemann Pick type C1 (NPC1)-like phenotype characterized by accumulation of cholesterol in lysosomes. Interestingly, NPC1 mRNA levels were specifically reduced by MPP^+. The decrease in NPC1 levels was also seen in midbrain and striatum from MPTP-treated mice and in primary cultures of neurons treated with MPP^+. Together with the MPP^+-dependent increase in intracellular cholesterol levels in N2a cells, we observed an increase in 5′ adenosine monophosphate-activated protein kinase (AMPK) phosphorylation and a concomitant increase in the phosphorylated levels of mammalian target of rapamycin (mTOR). NPC1 knockout delayed cell death induced by acute mitochondrial damage, suggesting that transient cholesterol accumulation in lysosomes could be a protective mechanism against MPTP/MPP^+ insult. Interestingly, we observed a negative correlation between NPC1 protein levels and disease stage, in human PD brain samples. In summary, MPP^+ decreases NPC1 levels, elevates lysosomal cholesterol accumulation and alters mTOR signaling, adding to the existing notion that PD may rise from alterations in mitochondrial-lysosomal communication.

1. Introduction

Cholesterol has a broad range of roles in the central nervous system. As an indispensable constituent of cell membranes, lipid rafts and myelin sheets, it is crucial for neurite outgrowth, dendritic spine maintenance, and synaptic function [1]. Although disruption in cholesterol metabolism has been associated with neurodegenerative disorders such as Alzheimer's and Huntington's disease, its role in Parkinson's disease (PD) is still debatable. PD is the second most common aged associated neurodegenerative disease, characterized by motor symptoms, as a consequence of the progressive loss of dopaminergic neurons in the Substantia Nigra pars compacta (SNpc) [2]. Research conducted on the brains of individuals with Parkinson's disease reveals a decrease in mitochondrial complex I activity, elevated generation of reactive oxygen species (ROS), and an inadequate antioxidant capacity. These findings indicate that mitochondrial dysfunction plays a vital role in the progression of neurodegenerative processes. [3,4]. Furthermore, the use of mitochondrial complex I inhibitors, including rotenone, 1-methyl-4-phenyl-1,2,3,6-tetrahydropyridine (MPTP), and its toxic metabolite 1-methyl-4-phenylpyridinium (MPP^+), triggers a series of events that result in parkinsonism and the development of neuropathological characteristics observed in both humans and animal models of

* Corresponding author at: Faculty of Pharmacy, Universidade de Lisboa, Av. Prof. Gama Pinto, 1649-003 Lisbon, Portugal.
E-mail address: Elsa.Rodrigues@ff.ulisboa.pt (E. Rodrigues).

https://doi.org/10.1016/j.bbadis.2023.166980
Received 9 June 2023; Received in revised form 13 November 2023; Accepted 28 November 2023
Available online 5 December 2023

the disease [5–9].

While the correlation between the disturbance of cholesterol homeostasis and neurodegeneration is well-established, the direct impact on mitochondrial function has only been demonstrated more recently. Mitochondrial cholesterol loading is a pivotal factor in the pathogenesis of various neurological disorders linked to mitochondrial dysfunction, such as Alzheimer's and Niemann Pick type C (NPC) disease. The deleterious effects of mitochondrial cholesterol accumulation involve the disruption of the mitochondrial membrane's physical properties, which hinders the transportation of glutathione into the mitochondrial matrix, consequently compromising antioxidant defences (for review see [10]).

These studies underline the role of cholesterol in mitochondrial function; nevertheless, the impact of defective mitochondria on cholesterol homeostasis has not been fully addressed. Since mitochondria act as signaling platforms, linking metabolism to cellular bioenergetics and cell fate, and since this organelle can regulate lysosomal function, it is plausible that they may also disturb cholesterol metabolism and intracellular trafficking. Interestingly, genome-wide association studies have pinpointed *SREBF1* as a genetic risk locus for PD [11], while a genome-wide RNAi screen identified the protein encoded by *SREBF1*, the sterol-responsive element binding protein 1 (SREBP1), as a regulator of the PTEN-induced kinase 1 (PINK1)/parkin mitophagy pathway [12]. In rodents, the identification of *Srebf1* as a vital transcriptional regulator in midbrain dopaminergic neurogenesis suggests that interventions targeting the levels or function of SREBP1 could potentially serve as valuable therapeutics. These interventions may help prevent the loss of midbrain dopaminergic neurons or facilitate the generation of new ones, offering potential benefits for cell replacement therapy in Parkinson's disease (PD) [13]. In line with this, a decrease in cholesterol synthesis is suggested to be involved in PD [14]. While parkin, an E3 ubiquitin ligase encoded by *PARK2*, which is mutated in patients suffering from early onset familial forms of PD, regulates systemic lipid metabolism, the modulation of cholesterol biosynthesis controls parkin expression [15]. Interestingly, in single-cell transcriptomics of human iPSC-derived dopaminergic neurons, Fernandes and collaborators, found a population of dopaminergic neurons with an expression pattern similar to the one observed in human adult dopaminergic neurons, that presented an upregulation in the expression levels of cholesterol biosynthesis genes, in comparison with other neuronal populations [16]. The authors also observed a downregulation of cholesterol biosynthesis genes in these dopaminergic neurons in response to oxidative stress, endoplasmic reticulum (ER) stress, and the SNCA-A53T mutation.

Here we aimed to investigate how mitochondrial dysfunction may affect neuronal cholesterol homeostasis, and identify potential disease-modifying targets in the context of PD. In this study, we show that inhibition of mitochondrial complex I in neuronal cells results in a decrease in NPC1 expression, and the simultaneous build-up of cholesterol within lysosomes. Thus, our results support former reports that highlight common pathways between PD and lysosomal storage disorders [17].

2. Materials and methods

2.1. Reagents and supplements

Dulbecco's Modified Eagle Medium (DMEM), Eagle's Minimum Essential Medium (MEM), Ham's F-12 1× Medium and Fetal Bovine Serum (FBS) were purchased from Corning (Life Sciences, MA, USA). Opti-Minimum Essential Medium (Opti-MEM), MEM Non-Essential Amino Acids Solution 100×, Hank's balanced salt solution (HBSS), penicillin-streptomycin solution, L-glutamine, 0.05 % trypsin solution, Neurobasal medium, B27 supplement, gentamicin and TripLE Express were acquired from Gibco® (Thermo Fisher Scientific Inc., MA, USA). Thiazolyl Blue Tetrazolium Bromide used in MTT viability assay, L-glutamic acid, poly-d-lysine, Amido Black Staining Solution 2×, Filipin III from *Streptomyces filipinensis*, carbonyl cyanide 3-chlorophenylhydrazone (CCCP), 1-methyl-4-phenyl-1,2,3,6-tetrahydropyridine (MPTP) and 1-methyl-4-phenylpyridinium (MPP^+), antimycin A and oligomycin were bought from Merck (Sigma Aldrich Inc., MO, USA). Proteinase inhibitors, DNAse I Recombinant Kit, Cytotoxicity Detection Kit PLUS (LDH) and β-galactosidase Reporter Gene Assay (chemiluminescent) were purchased from Roche Applied Science (Penzberg, Germany). Bovine serum albumin (BSA), polyvinyl difluoride (PVDF) membranes and SuperSignal™ West Femto were obtained from Thermo Fisher Scientific Inc. 30 % Acrylamide/Bis-acrylamide and Bio-Rad Protein Assay Reagent were obtained from BioRad Laboratories Inc. (CA, USA). Sodium dodecyl sulfate (SDS) 20 % and NZYTech Reverse Transcriptase Kit was acquired from NZYTech Lda (Lisbon, Portugal). Lipofectamine 3000 and Amplex Red Cholesterol Assay Kit were purchased from InvitrogenTM (Thermo Fisher Scientific Inc). NucSpot 470 Nuclear Stain and ATP-GloTM Bioluminometric Cell Viability Assay Kit were obtained from Biotium (CA, USA). WesternBright™ ECL was purchased from Advansta (CA, USA). TRIzol Reagent was bought from Ambion (Thermo Fisher Scientific Inc., USA).

2.2. Antibodies

The primary antibodies used in Western Blot analysis were purchased as follow: rabbit anti-mTOR (Cat. #2972), rabbit anti-p-mTOR (Ser2448) (Cat. #2971), rabbit anti-AMPKα (Cat. #2532) and rabbit anti-pAMPKα (Thr172) (Cat. #2535) from Cell Signaling Technology Inc. (MA, USA); rabbit anti-p70S6K (Cat. #AF8962), rabbit anti-pp70S6K (T421/S424) (Cat. #AF8965) from R&D Systems (MN, USA) and rabbit anti-NPC1 form Novus Bio (Cat. #NB400-148). The goat anti-rabbit horseradish peroxidase (Cat. #1706515) secondary antibody, was acquired from BioRad Laboratories Inc. For the immunocytochemistry assays, the primary antibody rat anti-LAMP2 (Cat. #sc19991) was acquired from Santa Cruz Biotechnology Inc. (Dallas, TX, USA), whereas the secondary goat anti-rat Alexa Fluor 594 was obtained from Thermo Fisher Scientific Inc.

2.3. Animal treatments and dissection

Animal experiments were conducted under the Institutional Portuguese and European guidelines (Diário da República, n.° 151/2013, Série I de 2013-08-07; and 2010/63/EU European Council Directive), and approved by the Direção Geral de Alimentação e Veterinária and Órgão Responsável pelo Bem-Estar Animal (ORBEA) of the Faculty of Pharmacy, Universidade de Lisboa (License nr 1885/2021). Male C57BL/6 wild-type mice, aged twelve weeks, were acquired from Harlan. Mice were maintained under controlled conditions, including a 12-h light-dark cycle, constant temperature (22–24 °C), humidity (50–60 %), and provided *ad libitum* access to standard diet and water, in the FFU-Lisboa Animal House – Campus Lumiar. The animals were separated into three groups depending on the treatment regimen. Animals treated with MPTP received a single acute i.p. injection of 40 mg/kg body weight and were later sacrificed 3 h or 6 h post-injection, whereas control mice were injected i.p. with a saline solution and were sacrificed 6 h after injection. All mice were anesthetized with isoflurane, decapitated, and the brains were collected and separated into hemispheres. One hemisphere was used for immunohistochemistry and was immediately fixed with 4 % paraformaldehyde and further processed for cryostat sectioning, while the midbrain and striatum brain regions were dissected as previously described [6–9], and frozen in liquid nitrogen.

2.4. Human brain samples

Human brain samples from Parkinson's disease patients and matched controls were obtained from The Netherlands Brain Bank (Project 1525-NBB; open access: www.brainbank.nl), following their ethical guidelines. All material was collected from donors from whom a written

consent for a brain autopsy and the use of material and clinical information for research purposes had been obtained by the NBB. Mesencephalon tissue samples of 4 PD patients (age range: 68–79; m/f: 3/1) and 4 control subjects (age range: 77–92; m/f; 2/2), obtained with a short *post-mortem* delay, were selected based on clinical diagnosis and confirmed by neuropathological evaluation. Control cases had no known clinical history of dementia or motor disturbance and the cause of death was unrelated to the central nervoussystem.

2.5. Cell culture and drug treatments

N2a mouse neuroblastoma cells were cultured at 37 °C and 5 % CO2 in humidified atmosphere, in 1:1 (v/v) Opti-MEM/high glucose DMEM media, supplemented with 10 % heat inactivated FBS, 2 mM L-glutamine, penicillin (100 U/mL) and streptomycin (100 μg/mL). For Western Blot and RT-qPCR analysis, cells were treated with vehicle or mitochondrial toxins for 6 or 16 h. MPP^+ was used in the concentrations of 250 μM or 1 mM, CCCP in 20 μM, antimimycin A in 1 μM and oligomycin in the dosage of 2 μM. For immunocytochemistry assays, cells were treated with vehicle, 1 mM of MPP^+ or 20 μM CCCP for 16 h. Quantification of intracellular cholesterol levels by Amplex Red was performed after treatment with vehicle or 100 μM, 250 μM and 1 mM MPP^+, or 10 μM and 20 μM CCCP for 6 and 24 h. ATP levels were measured in cells treated for 3 h with 100 μM, 250 μM, 500 μM and 1 mM MPP^+.

The SH-SY5Y human neuroblastoma cell line knockout for NPC1 was kindly offered by Dr. Daniel Grinberg, Universitat de Barcelona (SH-NPC). WT and NPC1 knockdown cells, were maintained in monolayer in 1:1 (v/v) Eagle's MEM/Hams F12 media, supplemented with 10 % heat inactivated FBS, 2 mM L-glutamine, penicillin (100 U/mL) and streptomycin (100 μg/mL). The positive selection was maintained by the addition of 500 μg/mL G418 Sulfate (Gibco®, Thermo Fisher Scientific Inc.), to the culture medium. Evaluation of cell death and viability was done after treating cells with vehicle or 500 μM, 1 mM and 2 mM of MPP^+ for 24 and 72 h.

Primary cultures of mouse cortical neurons were prepared from 15- to 17-day-old CD-1 mouse fetuses, as previously described [9,18]. Pregnant mice were sacrificed in a CO_2 chamber and the embryos were collected in HBSS with Ca^{2+} and Mg^{2+} and quickly decapitated. After removal of olfactory bulbs, white matter and meninges, the brain cortex was collected in HBSS without Ca^{2+} and Mg^{2+} (HBSS-2). The cortex was then mechanically fragmented, transferred into a 0.05 % trypsin solution, and incubated for 15 min at 37 °C. Following trypsinization, cells were washed twice with a solution of HBSS-2 and 10 % FBS, and subsequently resuspended in plating medium – Neurobasal medium supplemented with 2 % B27 supplement, 25 μM L-glutamic acid, 0.5 mM L-glutamine and 12 mg/mL gentamicin. Isolated neurons were plated with a density of 500–650 cells/mm^2 on culture plates pre-coated with poly-D-lysine and maintained at 37 °C in a humidified atmosphere of 5 % CO_2. Cells were maintained for 10 to 13 DIV before treatments. Half of the medium was renewed every 3–4 days, and glutamic acid was only added into the medium when plating the cells. All the subsequent media changes and cell treatments were free from glutamic acid.

2.6. Preparation of total protein cell and tissue extracts

For total protein cell extraction, after PBS washing, N2a cells were collected in lysis buffer (50 mM Tris-HCl pH 7.4, 180 mM NaCl, 1 mM EDTA, 1 % Triton-X100, 1 mM DTT, 10 mM NaF, 1.25 mM Na3VO4 and 1× protease inhibitors). Total protein extracts from mouse midbrain and striatum were prepared from a pool of two different MPTP-treated mice brains from the same experimental group, which were mixed, homogenized and resuspended in cell lysis buffer 1× (Cell Signaling Technology) supplemented with 1 mM DTT, 1.25 mM Na_3VO_4 and 1× protease inhibitors, as previously described [6–9]. Afterwards, the samples were subjected to four cycles of sonication, each lasting 4 s, and subsequently centrifuged at 13,000 ×*g* for 15 min at 4 °C. Protein concentration was quantified using the Bradford method (Bio-Rad Protein Assay Reagent). Total protein extracts from Human brain samples were prepared as described for mouse samples.

2.7. Western blot analysis

Total protein extracts from N2a cells or mouse midbrain and striatum were denatured for 5 min at 95 °C using a mixture of 1:1 (v/v) sample/2× SDS sample buffer (0.25 M Tris-HCl pH 6.8, 4 % SDS, 4 % glycerol, 1 % β-mercaptoethanol and bromophenol blue). Afterward, proteins were resolved on 7.5 % or 10 % SDS-polyacrylamide (37.5:1 crosslinker ratio) gel electrophoresis (SDS-PAGE) and transferred to a PVDF membrane. For immunodetection, the membranes were blocked in 5 % dry non-fat milk in Tris-buffered saline-tween (TBS-T, 20 mM Tris-HCl pH 7.6, 150 mM NaCl, 0.1 % Tween-20) for 1 h and incubated overnight at 4 °C (with agitation in a cold chamber) with the specific primary antibodies: rabbit anti-*p*-mammalian target of rapamycin (mTOR) (1:500 5 % BSA in TBS-T), rabbit anti-mTOR (1:1000 5 % BSA in TBS-T), rabbit anti-*p*-AMPK α (1:1000 3 % BSA in TBS-T), rabbit anti-AMPKα (1:1000 5 % BSA in TBS-T), rabbit anti-*p*-protein S6 kinase beta-1 (p70S6K) (1:1000 3 % BSA in TBS-T), rabbit anti-p70S6K (1:1000 5 % BSA in TBS-T) and rabbit anti-NPC1 (1:1000 5 % BSA in TBS-T), After rinsing with TBS-T, membranes were incubated with goat anti-rabbit secondary antibody, conjugated with horseradish peroxidase (1:5000 5 % non-fat dry milk) in TBS-T for 1 h at room temperature with agitation. The immunocomplexes were visualized by chemiluminescence detection using WesternBright™ ECL or SuperSigmal™ West Femto reagents in ChemiDoc™ MP Imaging System (Bio-Rad, USA). The amido Black staining was used as loading control. Results were analysed using Image Lab Software Version 5.0 build 18 (Bio-Rad Laboratories, USA) and are displayed as fold induction from control samples.

2.8. Isolation of total RNA

Total RNA was isolated from N2a cells and from midbrain and striatum samples of control and MPTP-treated animals, using the TRIzol reagent. Briefly, cells and brain tissue were lysed in TRIzol Reagent and incubated at room temperature for 5 min. For each mL of TRIzol used, 0.2 mL of chloroform was added. Then, samples were vigorously agitated for 15 s, incubated 2 to 3 min at room temperature and centrifuged at 12,000 ×*g* for 15 min at 4 °C. The aqueous phase was recovered, and RNA was precipitated by adding 0.5 mL of isopropanol for each mL of TRIzol used, followed by an incubation for 10 min at room temperature. After centrifugation at 12,000 ×*g* for 10 min at 4 °C, the resulting pellet was washed with 70 % ethanol and airdried. Finally, the extracts were resuspended in nuclease-free water and incubated for 10 min at 55 °C. RNA was quantified in the Nanodrop spectrophotometer (Thermo Scientific, USA).

2.9. Quantitative polymerase chain reaction (RT-qPCR)

Firstly, 1 μg of RNA from each sample was digested with 0.1 U/μL DNAse I Recombinant enzyme for 20 min at 37 °C, followed by 10 min at 75 °C, in a VWR Thermal Cycler (VWR International LLC, USA). cDNA synthesis was performed with 5 ng/μL mM random hexamers, 0.5 mM dNTP mix and 5 U/μL of NZY Reverse Transcriptase enzyme (NZYTech), according to the manufacturer's instructions. The heating program was as follows: 10 min at 25 °C, 50 min at 50 °C, and 5 min at 85 °C.

For RT-qPCR, SensiFAST™ SYBR® Hi-ROX Kit (Bioline, UK) and specific primers for each target gene (Table 1) were used. The QuantStudio 7 Flex Real-Time PCR System (Thermo Fisher Scientific, USA) was used following a cycling program of an initial incubation of 2 min at 95 °C, and 40 cycles of 5 s at 95 °C and 20 s at 60 °C. Each sample was assayed in duplicate and the mRNA levels were normalized to the level of Eukaryotic elongation factor 1-alpha (Eef). Reference genes were

Table 1
Details of the mouse primers used for RT-qPCR.

Gene	Forward primer	Reverse primer	Ref.
Acat1	5′ GAAGGCTCACTCATTTGTCAGA 3′	5′ GTCTCGGTAAATAAGTGTAGGCG 3′	
ApoE	5′ CTTCTGGGATTACCTGCGCT 3′	5′ GTCCTCCATCAGTACCGTTCAG 3′	
Ctsd	5′ GCCTCCGGTCTTTGACAACTT 3′	5′ CACCAAGCATTAGTTCTCCTCC 3′	
Cyp46a1	5′ CGACGCCAGCCATTCCTCCTT 3′	5′ AGAGTCCCATAGCCAACCACAAGA 3′	
Eef	5′ ACACGTAGATTCCGGCAAGT 3′	5′ AGGAGCCTTTTCCCATCTC 3′	[20]
Hmgcr	5′ CCGGCAACAACAAGATCTGTG 3′	5′ ATGTACAGGATGGCGATGCA 3′	[21]
Hmgs	5′ GTCTCCTTGCTTTGCTCGTTC 3′	5′ GGACAGAGAACTGTGGTCTCC 3′	[22]
Lamp1	5′ GACGGTGACCAGAGCGTT C 3′	5′ GTGGGCACTAGGGCATCAG 3′	
Ldlr	5′ GAACTCAGGGCCTCTGTCTG 3′	5′ AGCAGGCTGGATGTCTCTGT 3′	[23]
Lipa	5′ TTTAGTCTTGGCTCCCGTG 3′	5′ CCAAACATGTCCTTGAGAAGAG 3′	
Lss	5′ CCCTGAACTATGTGGCTCT 3′	5′ ATAGGGTGTTGAGTCCTTCC 3′	
Mvk	5′ ATCGGTATTAAGCAGGTGTG 3′	5′ GATTGCCAGGTACAGGTAGA 3′	
Npc1	5′ TGGAGAGTGTGGAATTGCGAC 3′	5′ GGACACCTGGACAGG AACTG 3′	
Tfeb	5′ CCACCCCAGCCATCAACAC 3′	5′ CAGACAGATACTCCCGAACCTT 3′	[24]
Srebp2	5′ GCG TTC TGG AGA CCA TGG A 3′	5′ ACAAAGTTGCTCTGAAAACAAATCA 3′	[25]

selected using the NormFinder software [19] and results are presented as fold induction over controls, using the ΔΔCt method. Statistical analysis was performed using the ΔCt values.

2.10. Luciferase gene reporter assay

N2a cells were transfected with Lipofectamine 3000 using 2 μL of reagent *per* microgram of DNA. Cells were transfected with pLDLR-luciferase reporter plasmid [26] and CMV-β-galactosidase plasmid. The pLDLR-luciferase reporter plasmid contains the sterol responsive element (SRE) of the low lipoprotein receptor (LDLR) promotor upstream of the luciferase gene. N2a cells were plated at a density of 20,000 cells transfected with 50 ng of DNA in each well of a 96-well plate, in duplicates. Growth medium was replaced in the following day, and cells were treated as described above. After treatments, cells were washed with PBS and lysed in β-galactosidase reporter gene assay lysis buffer 1×. Luciferase and β-galactosidase activity were measured as previously described [27]. All readings were performed in FB 12 luminometer (Berthold Detection Systems, Germany). Normalization of the luciferase activity was based on β-galactosidase activity and results are presented as fold induction over control samples.

2.11. Amplex Red cholesterol assay

The Amplex Red Cholesterol Assay Kit was used according to the manufacturer's instructions. Specifically, cells were lysed in reaction buffer, sonicated four times for 4 s and centrifuged at 13,000 ×*g* for 10 min at 4 °C. In a 96-well plate, the recovered supernatant was diluted 10× in reaction buffer, to a final volume of 50 μL. In parallel, a cholesterol calibration curve and a negative control without cholesterol were prepared. Reaction was initiated with the addition of 50 μL of a solution containing 300 μM Amplex Red reagent, 2 U/mL horseradish peroxidase, 2 U/mL cholesterol oxidase and 0.2 U/mL cholesterol esterase in reaction buffer. To measure free cholesterol levels, 50 μL of the same solution but without cholesterol esterase was added to the samples. Each condition was assayed in duplicate. The levels of esterified cholesterol were obtained by subtracting the values of free cholesterol from total cholesterol levels. After incubation for 30 min at 37 °C, the microplate was read in GloMax Multi+ Detection System (Promega Corporation, USA) at 590 nm. The background fluorescence was corrected by subtracting the negative control and normalization of the results was obtained through protein quantification using Bio-Rad Protein Assay Reagent. The Amplex Red Cholesterol Assay kit was also used to quantify cholesterol levels in midbrain and striatum of control and MPTP-treated mice, using the total protein extracts previously described diluted 1:50 in reaction buffer 1×.

2.12. Immunocytochemistry

N2a cells were washed with PBS and fixed for 10 min at room temperature with 4 % paraformaldehyde in PBS. After, samples were rinsed and incubated with blocking solution (10 % fetal bovine serum, 0,05 % Tween-20 in PBS) for 45 min at room temperature. Incubation with the primary antibody anti-lysosomal-associated membrane protein 2 (LAMP2) (1:200 in blocking solution) was performed overnight at 4 °C, in a humid chamber. Then, the cells were washed with PBS and incubated for 2 h at room temperature with a cocktail of donkey anti-rat Alexa Fluor 594 secondary antibody (1:200), and 50 ng/μL Filipin III from *Streptomyces filipinensis*. After rinsing, nuclei were stained with NucSpot 470 Nuclear Stain in PBS for 30 min at room temperature. All images were acquired in an AxioScope.A1 microscope with an AxioCam HR camera (Zeiss, Germany), using 400× magnification in at least ten representative random fields. The time of exposure was set for treated samples. Quantification of total fluorescence and colocalization was performed with ImageJ 1.52i software (National Institutes of Health, USA) and results are shown as fold induction over control samples.

For free cholesterol staining, mice brain slices were dyed with filipin III (F4767, Sigma-Aldrich). Briefly, the slices were air-dried and rehydrated in phosphate buffer saline, and, posteriorly, 0.05 mg/mL filipin III in PBS 1x was added for 2 h in a humid chamber protected from light and at room temperature. The slices were then washed in phosphate buffer saline and mounted. Fluorescence visualization was performed in an AxioScope.A1 microscope with an AxioCam HRm camera.

2.13. ATP levels

Measurement of ATP levels was done using ATP-Glo™ Bioluminometric Cell Viability Assay Kit according to the manufacturer's protocol. ATP levels were measured in FB 12 luminometer, after adding 1:1 (v/v) of ATP-Glo detection cocktail (0.4 mg/mL D-luciferin, 1:100 (v/v) firefly luciferase in ATP-Glo assay solution) and sample, as previously described [28]. Each condition was assayed in triplicate. The results were normalized by accessing the amount of protein present by Bradford quantification using Bio-Rad Protein Assay Reagent and are expressed as fold induction over control samples.

2.14. MTT viability assay

The MTT viability assay was done according to MTT Assay Protocol for Cell Viability and Proliferation guidelines from Sigma Aldrich Inc. For this, after drug treatments, the reconstituted Thiazolyl Blue Tetrazolium Bromide solution was added to cells in a final concentration of 0.5 mg/mL, following incubation in a humidified atmosphere of 37 °C with 5 % CO_2 for 2 h. Then, the supernatant was removed, and the formazan crystals were dissolved in 100 μL of DMSO. Absorbance was

measured at 570 nm (reference value) and 620 nm (background value) using a Varioskan LUX Multimode Microplate Reader (Thermo Fisher Scientific Inc.). Results are presented as the percentage of viability which was calculated by subtracting the background from the reference values, and relative to the control samples. Each condition was assayed in triplicate.

2.15. LDH cytotoxicity assay

Evaluation of cell death was done by measuring the lactate dehydrogenase (LDH) levels in the supernatant using the Cytotoxicity Detection Kit PLUS. Accordingly, after the drug treatments, the culture supernatant was recovered and centrifuged at 250 ×*g* for 5 min to remove cell debris. A low control that contained only media and a high control that contained media with briefly lysed cells were also prepared. Each condition was assayed in triplicate. In a new 96-well plate, 50 μL of supernatant was mixed with 50 μL of the LDH assay solution and incubated at room temperature protected from light for 20 min. All absorbance readings were performed in Varioskan LUX Multimode Microplate Reader at 490 nm (reference value) and 690 nm (background value). Results are represented as percentage of cytotoxicity relative to the high control sample (lysed cells).

2.16. Statistical analysis

Data comparisons were evaluated using unpaired Student's *t*-test or Mann-Whitney test or Wilcoxon Signed Rank Test in case of non-parametric data. Additionally, one-way analysis of variance (ANOVA) followed by *post hoc* Tukey's or Dunnett's multiple comparisons test, and Kruskal-Wallis test followed by Dunn's for non-parametric data were also used for the statistical analysis. Analyses and graphics were performed using GraphPad Prism software version 9.0. (GraphPad Software Inc., San Diego, CA, USA). Results correspond to mean values ± standard error of the mean (SEM) and values of $p < 0.05$ were considered statistically significant.

3. Results

3.1. Effect of mitochondrial toxins on cholesterol homeostasis in neuronal cells

To determine if mitochondrial dysfunction affects cellular cholesterol homeostasis, we used N2a neuroblastoma cells treated with two mitochondrial toxins: MPP^+ and CCCP (Fig. 1). The MPP^+ mode of action parallels the mitochondrial dysfunction observed *post-mortem* in brains of PD patients, by blocking the multi-subunit enzyme NADH-ubiquinone oxidoreductase in the complex I of the electron transport chain. This causes a decrease in mitochondrial oxidative phosphorylation and an increase in oxidative stress [29]. CCCP functions as a powerful mitochondrial uncoupling agent, enhancing proton permeability across the inner membrane of the mitochondria. This, in turn, leads to the dissipation of the transmembrane potential and subsequent depolarization of the mitochondria [30].

Treatment of N2a cells with 1 mM MPP^+ led to a significant increase in the levels of total and free cholesterol after 6 ($p < 0.01$) and 24 h ($p < 0.05$) (Fig. 1A), whereas treatment with CCCP did not affect cholesterol accumulation at the same time points (Fig. 1B). Consequently, distinctive types of mitochondrial damage result in specific outcomes regarding intracellular cholesterol build-up, with the administration of MPP^+ causing a swift elevation in cholesterol levels.

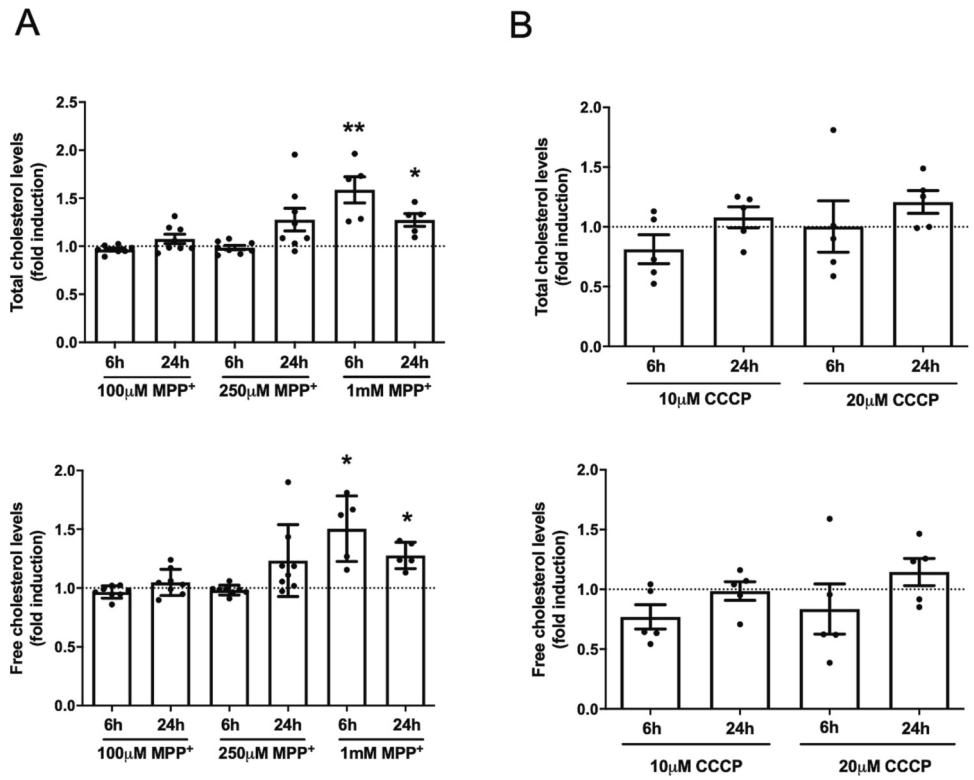

Fig. 1. MPP^+ treatment increases cholesterol levels in N2a neuroblastoma cells. Quantification of total (upper panel) and free cholesterol (lower panel) in N2a neuroblastoma cells treated with vehicle or 100 μM, 250 μM and 1 mM MPP^+ (A), or 10 μM and 20 μM CCCP (B) for 6 and 24 h. Cholesterol levels were determined in duplicates using the Amplex Red cholesterol assay. The results are expressed as fold induction over vehicle-treated cells and represent mean values ± SEM obtained from at least five independent experiences. Statistical analysis was performed by one-way ANOVA followed by Dunnett's multiple comparisons test (*$p < 0.05$; **$p < 0.01$).

3.2. MPP^+ reduces NPC1 expression in neuronal cells

In situations of energy crisis, anabolic pathways such as cholesterol biosynthesis are often repressed. Since MPP^+ treatment caused an overall increase in cholesterol levels in N2a neuroblastoma cells, we assessed if this could be due to an increase in cholesterogenic gene expression, by directly affecting SREBP2 mRNA expression levels, or by altering cholesterol uptake, efflux or intracellular trafficking. To that end, we treated N2a cells with 1 mM MPP^+ for 16 h and quantified the mRNA levels of *ApoE*, *Srebf2,* and its canonical target genes *Hmgcs1, Hmgcr*, *Ldlr*, and *Npc1* by RT-qPCR (Fig. 2). In addition, to gain a deeper comprehension of the impact of mitochondrial damage on cholesterol accumulation, we also treated cells with 20 μM CCCP, and with other compounds that mimic mitochondrial oxidative defects such as 1 μM antimycin-A, which inhibits complex III [31], and 2 μM oligomycin, which blocks ATP synthase [32].

Results presented in Fig. 2 show that the mRNA levels of *Srebf2* were significantly reduced by all the compounds tested, including MPP^+ (15 %), antimycin-A (35 %), oligomycin (50 %), and CCCP (50 %). The mRNA levels of the SREBP2 target genes *Hmgcs*, *Hmgcr* and *Ldlr*, were also significantly and concomitantly decreased by the mitochondrial toxins MPP^+, antimycin-A, and oligomycin. Although our results showed a clear trend, CCCP did not lead to a significant decrease in the mRNA levels of these genes. ApoE expression was only significantly reduced by antimycin-A. Interestingly, the mRNA levels of NPC1, that mediates cholesterol export from lysosomes and is implicated in the lysosomal storage disease Niemman-Pick type C disease [33], were specifically decreased by MPP^+ to approximately 50 % of control levels ($p < 0.01$).

3.3. MPP^+ treatment leads to lysosomal cholesterol accumulation in neuronal cells

Impaired egress resulting from loss-of-function mutations in either the NPC1 or NPC2 genes leads to the accumulation of unesterified cholesterol in late endosomes/lysosomes, ultimately causing lysosomal dysfunction and neuronal cell death [33]. Since our results showed that MPP^+ leads to a decrease in *Npc1* transcripts, we assessed if there were any changes in intracellular cholesterol distribution. N2a cells treated with MPP^+, antimycin A, oligomycin, and CCCP were labeled with filipin III together with immunocytochemistry for LAMP2 (Fig. 3). Filipin III, derived from *Streptomyces filipinensis*, is a natural fluorescent antibiotic that exhibits specific affinity for free cholesterol. Its binding properties enable the visualization of cholesterol accumulation patterns in cells. [34]. Overlapping this signal with the LAMP2 immunocytochemistry pattern allowed us to determine if cholesterol was sequestered in lysosomes.

Interestingly, MPP^+ treatment increased filipin III fluorescence per cell, to approximately 1.5-fold relative to control values ($p < 0.001$), reflecting an increase in free cholesterol levels (Fig. 3B). In contrast, the other compounds did not affect free cholesterol accumulation. Furthermore, treatment with mitochondrial toxins did not significantly affect LAMP2 immunocytochemistry patterns, but the relative LAMP2 fluorescence doubled in CCCP-treated cells (Fig. 3C).

Co-localization analysis of filipin III and LAMP2 immunofluorescence signals showed that although there was no overall redistribution of cholesterol in the cell (Fig. 3D1), there was a 1.4-fold increase in free cholesterol detected in lysosomes (Fig. 3D2). These results corroborate those depicted in Fig. 1 and indicate that the observed increase in cholesterol levels is due to its accumulation in lysosomes. As a positive control, we have used U18666A. U18666A is a compound that can mimic the accumulation of unesterified cholesterol in late-endosomal/lysosomal compartments similar to that occurring in NPC1-deficient cells (Supplementary Fig. 1).

Drug-induced impairment of mitochondrial function has been shown to elicit stress signaling pathways that regulate lysosome biogenesis that could mediate the observed increase in lysosomal cholesterol levels [35]. Therefore, we evaluated by RT-qPCR analysis the mRNA levels of

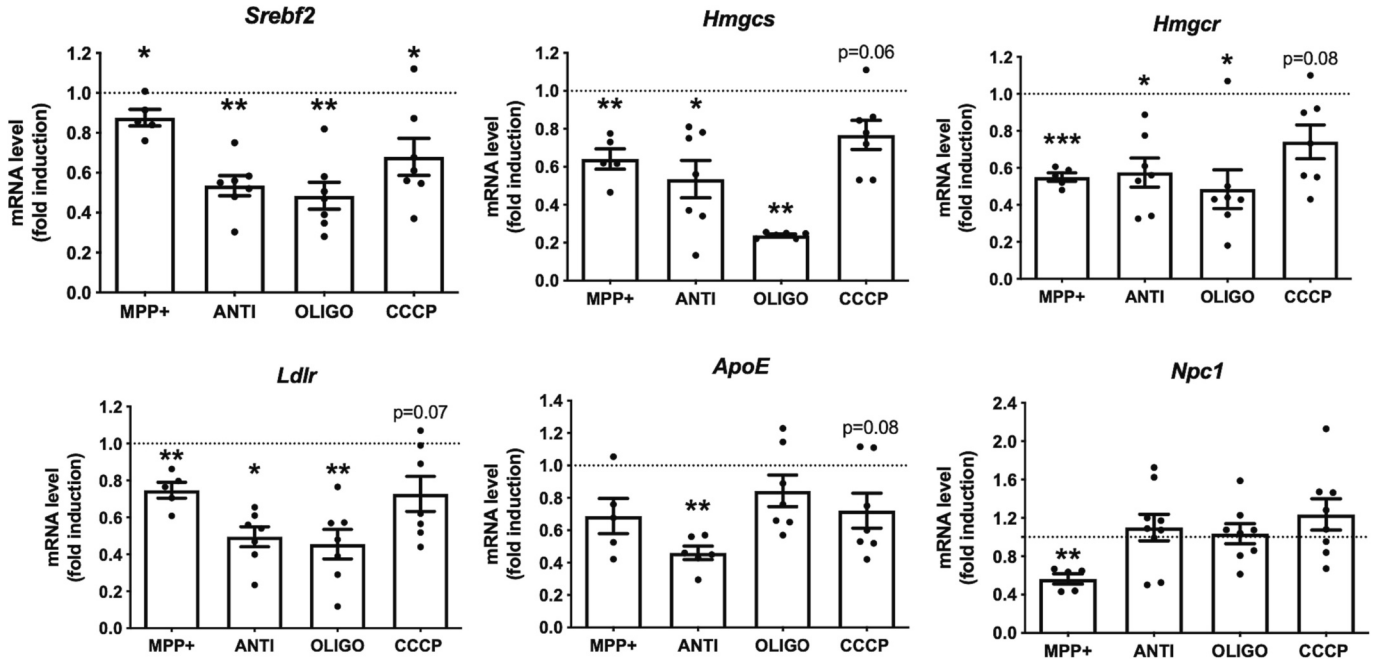

Fig. 2. MPP^+ reduces NPC1 mRNA levels in N2a neuroblastoma cells. RT-qPCR analysis of the mRNA levels of genes involved in biosynthesis (*Srebf2*, *Hmgcs*, and *Hmgcr*), efflux (*ApoE*), uptake (*Ldlr*) and intracellular cholesterol transport (*Npc1*), in N2a neuronal cells treated with different mitochondrial toxins. N2a neuroblastoma cells were treated 1 mM MPP^+, 1 μM antimycin A (ANTI), 2 μM oligomycin (OLIGO) or 20 μM CCCP for 16 h. Samples were assayed in duplicate and values were normalized to the internal standard *Eef*. Data is represented as mean values ± SEM from at least five individual experiments and is expressed as fold change over control. Statistical analysis was performed by Student's *t*-test for MPP^+ and one-way ANOVA followed by Dunnett's multiple comparisons test for ANTI, OLIGO and CCCP treatments (*$p < 0.05$; **$p < 0.01$; ***$p < 0.001$ *vs* vehicle treated cells).

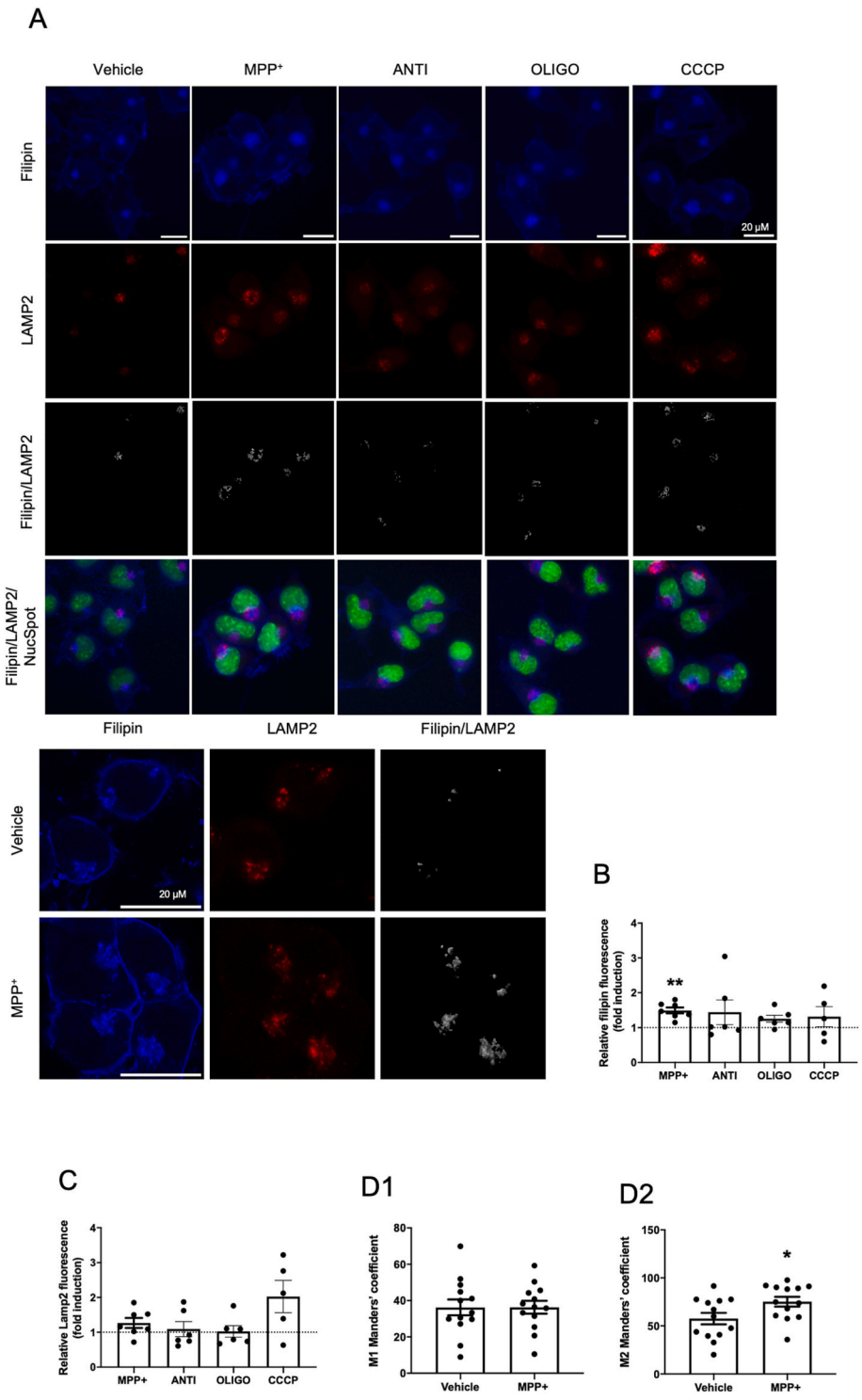

Fig. 3. MPP^+ treatment induces unesterified cholesterol accumulation in the late endosome/lysosome pathway. A) N2a neuroblastoma cells were treated with vehicle, 1 mM of MPP^+, 1 μM antimycin A (ANTI), 2 μM oligomycin (OLIGO) or 20 μM CCCP for 16 h. After fixation, cells were labeled with filipin III and NucSpot, and immunostained with LAMP2. Images are representative of filipin III (blue), LAMP2 (red) and nuclei (green), and co-localized pixels of LAMP2 with filipin III (white). In the lower panel higher magnification images are shown. Scale bar: 20 μm. The quantification of relative fluorescence for filipin III (B) and LAMP2 (C) was done using the values of average fluorescence normalized to total cell number. Results are represented as mean values ± SEM from at least four individual experiments and is expressed as fold change over control. D) Colocalization was determined using Mander's co-occurrence values from JaCoP plugin in ImageJ software (National Institutes of Health, USA). Data is represented as fold induction from control samples in mean values ± SEM, from fourteen independent experiences. (*$p < 0.05$; **$p < 0.01$). Statistical analysis was performed by Kruskal Wallis followed by Dunn's multiple comparisons test (B and C) or by Student's *t*-test (D). (For interpretation of the references to colour in this figure legend, the reader is referred to the web version of this article.)

Tfeb, and TFEB-lysosomal target genes in N2a neuroblastoma cells treated with vehicle or with the mitochondrial drugs for 16 h (Fig. 4). As TFEB targets, we selected lysosomal-associated membrane protein 1 (*Lamp1*), the lysosomal protease cathepsin D (*Ctsd*) and lipase A lysosomal acid type (*Lipa*). We observed a reduction of approximately 50 % in *Tfeb* mRNA levels in cells treated with MPP^+, suggesting a decrease in lysosomal biogenesis ($p < 0.05$). However, at least at this time-point, *Ctsd* mRNA levels in the same samples were 1.5-fold higher than in controls ($p < 0.05$). Our results also show that oligomycin significantly reduced *Lipa* mRNA levels ($p < 0.001$).

In agreement with our previous results, we show that different mitochondrial drugs used to induce mitochondrial oxidative defects lead to different cellular outcomes in terms of intracellular cholesterol accumulation. Indeed, concomitantly to its effect on the downregulation of NPC1, MPP^+ treatment leads to an increase in cholesterol accumulation in lysosomes.

3.4. MPP^+ leads to AMPK activation and decreased SREBP2 activity

Our results suggest that mitochondrial dysfunction induced by MPP^+ leads on one hand to a reduction in cholesterogenic gene expression, and on the other hand to an increase in intracellular cholesterol levels, likely due to its accumulation in the *endo*-lysosomal pathway. The mutual dependence between mitochondria and lysosomes is emphasized by numerous lines of evidence. For instance, it has been shown that under acute mitochondrial stress, AMPK is activated and results in mTORC1 inhibition [36]. In addition to the interaction with mTORC1, AMPK directly phosphorylates and negatively regulates HMGCR, the rate limiting enzyme in the cholesterol synthesis pathway [37]. The AMPKα subunit also associates with the precursor and nuclear forms of SREBP1 or SREBP2 isoforms to inhibit their activity [38]. Moreover, in NPC disease, loss of NPC1 function induces cholesterol build-up within lysosomes, resulting in hyperactivation of mTORC1, impaired mitochondrial function, and subsequent neurodegeneration [39].

Although the role of NPC1 loss-of-function mutations on aberrant cholesterol-mTORC1 signaling has been investigated [39], the effect of MPP^+-dependent downregulation of NPC1 on mTORC1 activity has not been addressed. Thus, we focused on investigating the activation of the AMPK/mTOR signaling pathway, given its importance in regulating lipid metabolism, and because its activation has been described within the context of PD [40–44].

To confirm that MPP^+ leads to a rapid decrease in cellular energy levels in N2a cells, we treated cells with vehicle or with increasing concentrations of MPP^+ for 3 h, and measured ATP levels (Fig. 5A). As expected, we observed a dose-dependent decrease in ATP levels, reaching up to 50 % in cells treated with 1 mM MPP^+. Western Blot analysis was used to determine the phosphorylation levels of AMPK (Fig. 5B). We observed an early and transient increase in AMPK phosphorylation after MPP^+ treatment. Indeed, when neuronal cells were treated with 1 mM MPP^+ for 6 h, the ratio between phosphorylated (*p*-AMPK) and total AMPK protein was increased by approximately 3.5-fold ($p < 0.05$), while no changes were detected after 16 h of MPP^+ treatment, when compared with vehicle-treated cells.

As mentioned before, the expression of cholesterogenic genes is under the strict control of the endoplasmic reticulum membrane-bound transcription factor SREBP2. SREBPs require a two-step proteolytic cleavage to generate a smaller active form, capable of entering the nucleus and binding to sterol regulatory elements (SRE) sequences in the promoters of the target genes [45]. To investigate if MPP^+ treatment leads to changes in the transcriptional activity of SREBP, we performed a reporter gene assay using the pLDLR-luc plasmid, which contains the SRE-sequence of the LDLR promoter upstream of the luciferase gene [26]. N2a cells were transfected with the pLDLR-luc reporter plasmid and 24 h after treated with vehicle or 250 μM MPP^+, for 24 h (Fig. 5C). We observed a significant decrease in luciferase activity after MPP^+ treatment (approximately 55 %; $p < 0.001$), suggesting a decrease in SREBP2 transcriptional activity which correlates with the decrease in the mRNA levels of SREBP2 target genes involved in cholesterol

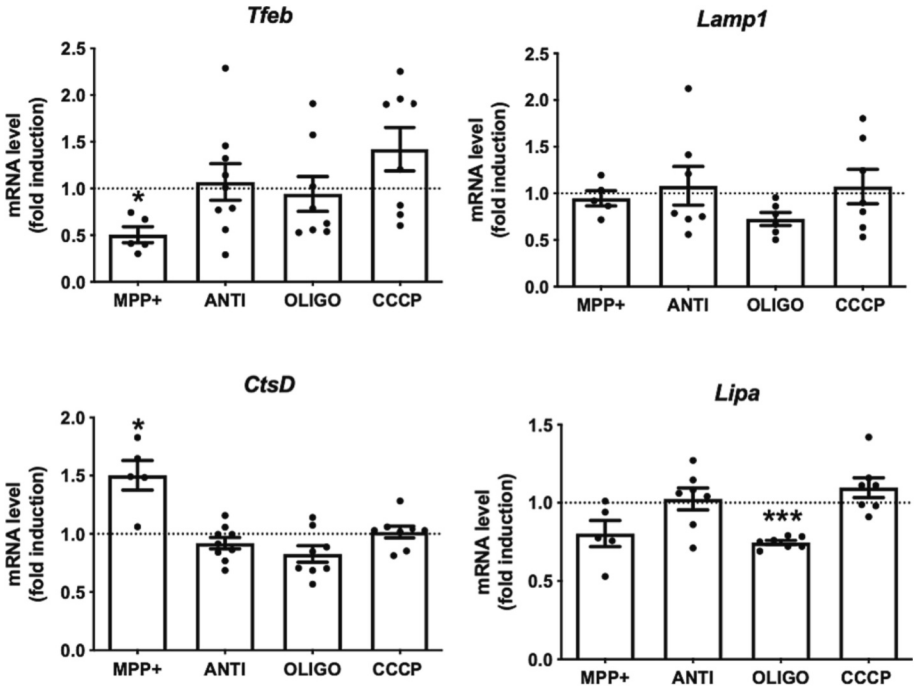

Fig. 4. MPP^+ treatment leads to changes in the expression levels of genes involved in late endosomes/lysosome pathways in N2a neuroblastoma cells. RT-qPCR analysis of the mRNA levels of genes involved in LE/LY pathway (*Lamp1*, *Tfeb*, *Lipa* and *CtsD*), in N2a neuronal cells treated with vehicle, 1 mM MPP^+, 1 μM antimycin A (ANTI), 2 μM oligomycin (OLIGO) or 20 μM CCCP for 16 h. Samples were assayed in duplicate and values were normalized to the internal standard *Eef* (eukaryotic translation elongation factor). For the mRNA analysis Student's t-test was performed for MPP+ and one-way ANOVA followed by Dunnett's multiple comparisons test for ANTI, OLIGO and CCCP treatments (*$p < 0.05$; ***$p < 0.001$ *vs* vehicle treated cells).

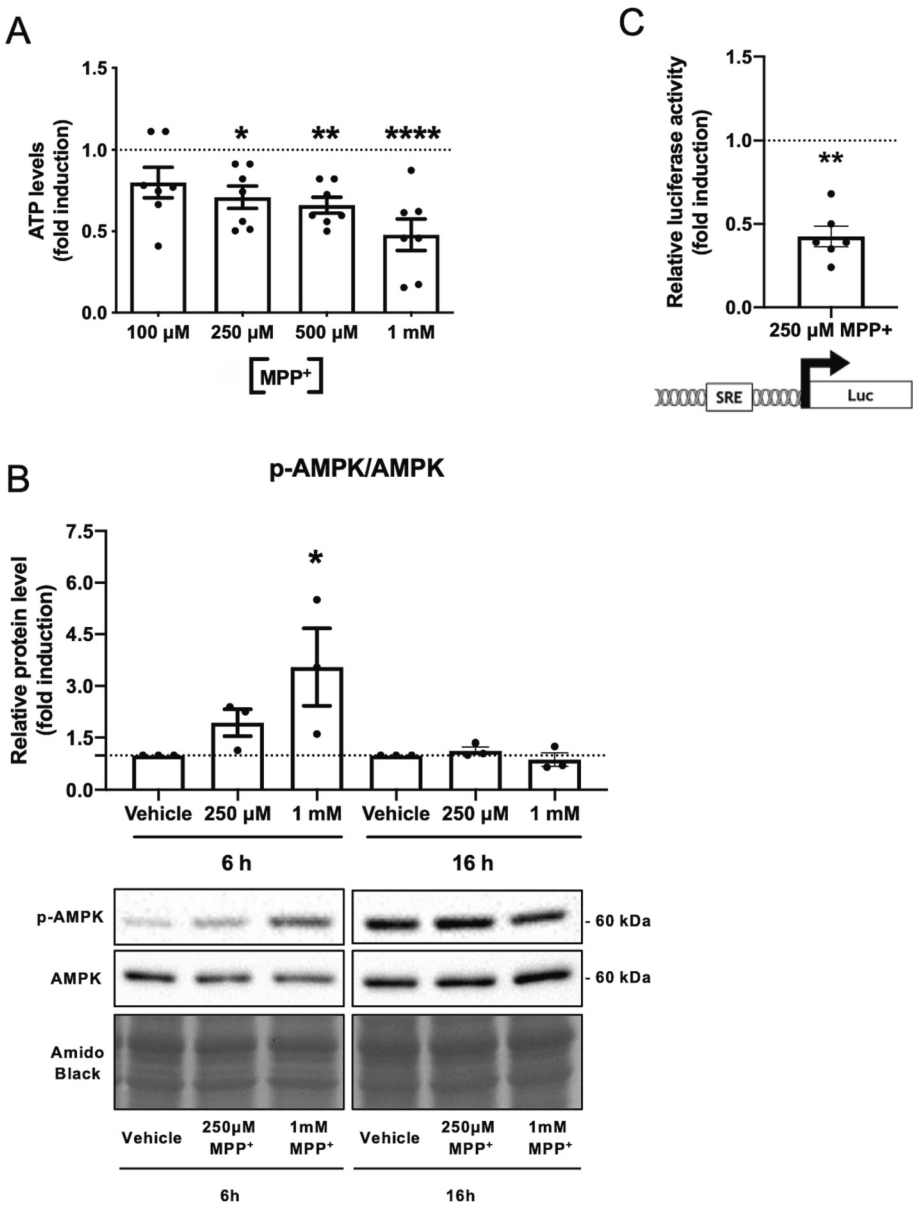

Fig. 5. MPP^+ triggers AMPK signaling pathway activation and represses SREBP2 transcriptional activity. A) ATP levels analysis of N2a neuronal cells treated with 100 µM, 250 µM, 500 µM or 1 mM of MPP^+ for 3 h. ATP levels were determined using the ATP Assay Kit and normalized using total protein values. Each condition was assayed in triplicate. Results are presented as mean values ± SEM of seven different experiments. Statistical analysis was performed by one-way ANOVA followed by Dunnett's multiple comparisons test (*$p < 0.05$). B) Western Blot analysis of p-AMPK/AMPK protein levels ratio after treatment with vehicle or 250 µM or 1 mM of MPP^+ for 6 or 16 h. In the lower panel are representative immunoblots for p-AMPK, AMPK and Amido Black staining. Data is represented as fold induction from vehicle-treated cells and is expressed as mean values ± SEM of three different experiments. Statistical analysis was performed by Kruskal Wallis followed by Dunn's multiple comparisons test (*$p < 0.05$). C) Relative *Srebp2* promoter activity in N2a neuronal cells treated with 250 µM MPP^+ for 24 h. Cells were transfected with pLDLR-luciferase plasmid, containing the luciferase coding-gene downstream to the SRE-sequence of the LDLR promoter. Data is shown as fold induction over the promoter activity in vehicle-treated cells, and normalized luciferase activities were expressed as mean values ± SEM of duplicates from six independent experiments. Statistical analysis was performed using the Wilcoxon Signed Rank Test (**$p < 0.01$).

synthesis and uptake (Fig. 2).

We next analysed the phosphorylation levels of mTOR, as well as the phosphorylation of p70 S6 Kinase, as a measure of mTORC1 activity (Fig. 6).

Interestingly, our results show a transient 1.6-fold increase in the p-mTOR/mTOR ratio 6 h after treatment with 1 mM MPP^+ (Fig. 6). Contrary to what was expected, we did not observe a concomitant increase in the phosphorylation levels of p70 S6 Kinase (Fig. 6). The cellular response to CCCP treatment, differed from MPP^+ since we did not observe any alteration in mTOR phosphorylation 6 h after treatment (Fig. 7B). Nevertheless, and as expected, we observe a 3.7 and 3-fold increase in p-AMPK/AMPK ratio 6 and 16 h after CCCP administration (Fig. 7A). Together, our results suggest that, in neuronal cells, MPP^+ leads to a decrease in SREBP transcriptional activity, either due to AMPK activation, or in response to the accumulation of cholesterol in lysosomes. Concomitantly, we observed an early and transient increase in the phosphorylation levels of mTOR.

3.5. *NPC1 knockout protects against MPP^+-induced cell death*

To understand if the decrease in NPC1 levels, induced by MPP^+ and MPTP treatment, might be a protective or a deleterious stress response

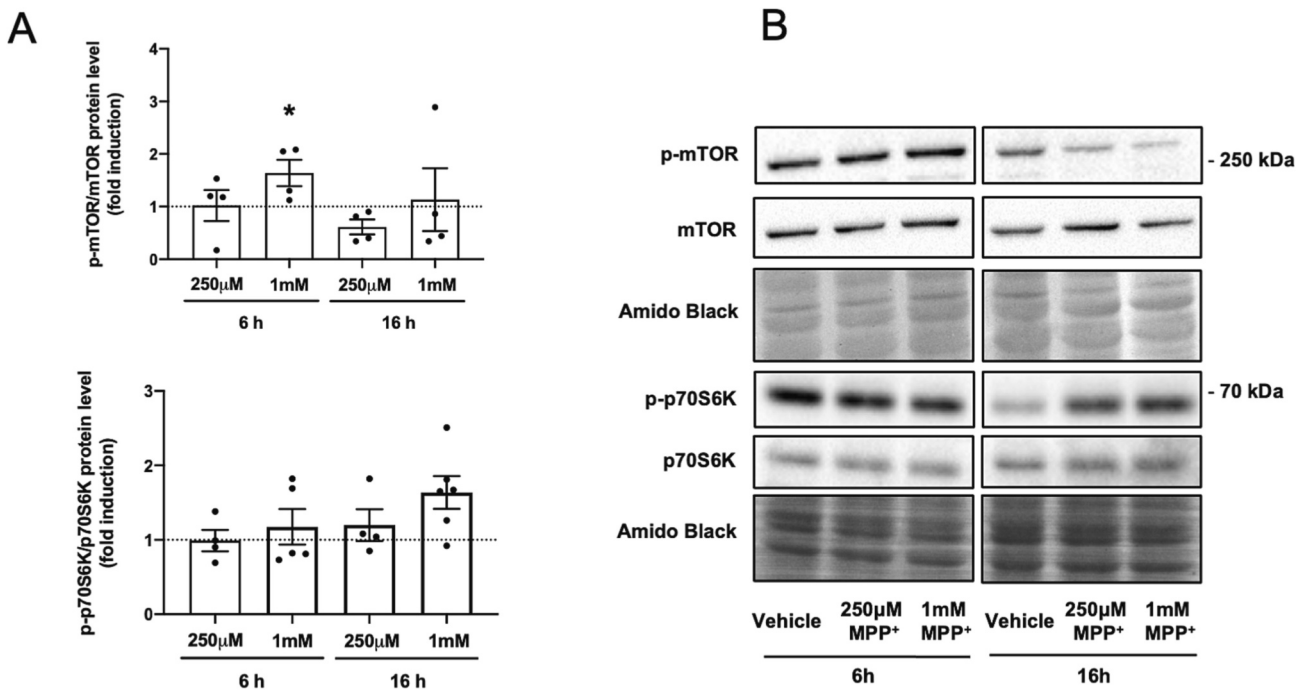

Fig. 6. N2a neuronal cells treated with MPP^+ show an early and transient induction of mTOR signaling. Western Blot analysis of p-mTOR/mTOR and p-p70/p70 protein levels ratio, after treatment with vehicle or 250 μM or 1 mM of MPP^+ for 6 or 16 h. (A) Results are shown as fold induction from vehicle treated cells and expressed as mean values ± SEM of at least three different experiments. (B) Representative immunoblots for p-mTOR, mTOR, p-p70, p70 and Amido Black staining, which was used as loading control. Statistical analysis was performed by Kruskal Wallis followed by Dunn's multiple comparisons test (*$p < 0.05$).

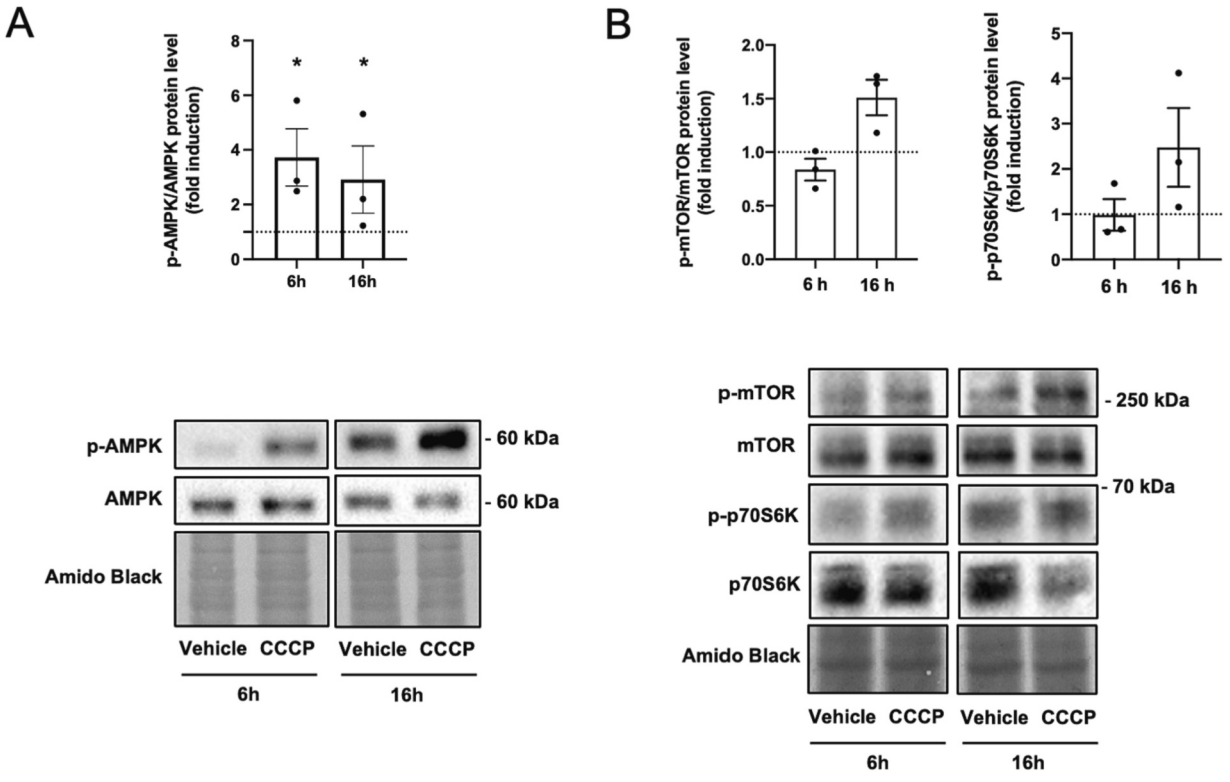

Fig. 7. N2a neuronal cells treated with CCCP show later activation of mTOR signaling. Western Blot analysis of (A) p-AMPK/AMPK protein levels ratio and (B) p-mTOR/mTOR and p-p70/p70 protein levels ratio, after treatment with vehicle or 20 μM CCCP for 6 h or 16 h. Lower panels show representative immunoblots for p-AMPK, AMPK, p-mTOR, mTOR, p-p70, p70 and Amido Black staining, which was used as loading control. Results are shown as fold induction from vehicle treated cells and expressed as mean values ± SEM of at least three different experiments. Statistical analysis was performed by Kruskal Wallis followed by Dunn's multiple comparisons test (*$p < 0.05$).

we used a neuronal SH-SY5Y cell line with NPC1 genetic deletion (SH-NPC).

Wild-type SH-SY5Y (SH-WT) and SH-NPC were treated with increasing concentrations of MPP^+ for 24 h followed by analysis of MTT reduction (Fig. 8A). In SH-WT cells we observed a significant decrease in MTT reduction of approximately 30, 40 and 57 %, in cells treated with 0.5, 1 and 2 mM MPP^+, respectively. Interestingly, in SH-NPC cells, treatment with 0.5 mM MPP^+ did not lead to any significant decrease in MTT reduction, while treatment with 1 and 2 mM MPP^+ decreased cell viability by 30 % and 40 %. These results show that when compared to SH-WT, SH-NPC cells require higher MPP^+ concentrations to undergo a similar reduction in cell viability.

To confirm that the NPC1 knock-out affects the cellular response to MPP^+ we further determined LDH release, as a measure of cell death. SH-WT and SH-NPC were treated with increasing concentrations of MPP^+ for 72 h and LDH release was determined (Fig. 8B). In SH-WT cells we observed a significant increase in LDH release of approximately 54 and 74 %, in cells treated with 1 and 2 mM MPP^+, respectively. Interestingly, in SH-NPC cells, treatment with either 0.5 or 1 mM MPP^+ did not lead to increased LDH release, while treatment with 2 mM MPP^+ did (42 %). This further shows that SH-NPC cells are more resistant to MPP^+-induced cell death compared to SH-WT.

These results suggest that the transient intracellular cholesterol accumulation observed after MPP^+ treatment might be a protective cellular mechanism triggered in response to mitochondrial damage, hampering the activation of signaling pathways that activate cell death mechanisms.

3.6. *NPC1 levels are decreased in the striatum and midbrain of MPTP-treated mice*

Taking in consideration the changes in cholesterol homeostasis elicited by MPP^+ in N2a neuroblastoma cells, we investigated if similar alterations could be observed in an *in vivo* model of PD. Accordingly, we firstly analysed whether MPTP was able to trigger cholesterol accumulation in samples of striatum and midbrain of mice treated with a single i.p. dose of 40 mg/kg MPTP or saline, and sacrificed 3 or 6 h after injection. The selected time points are due to the close temporal relationship that exists between the formation of MPP^+ - reaching its peak at 3 h following MPTP treatment - and the inhibition of mitochondrial respiration in the CNS by MPP^+ [46]. Nevertheless, we could not detect any change in the levels of total and free cholesterol (data not shown). This was not surprising, since small alterations in intracellular cholesterol levels are masked by bulk myelin-associated cholesterol in the CNS.

In agreement with our *in vitro* data, in the midbrain we could observe a time-dependent significant decrease in the levels of *Ldlr*, *Npc1* and *Lipa*

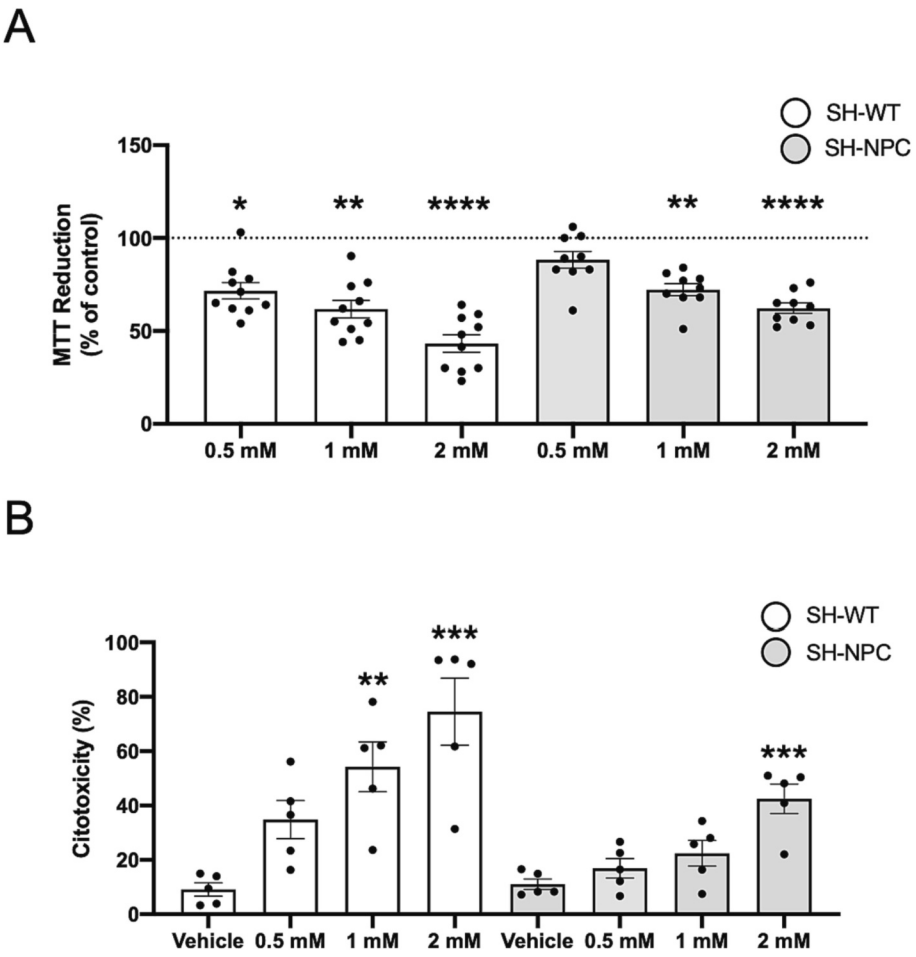

Fig. 8. NPC1 knock-out protects against MPP^+-induced cell death. SH-SY5Y cells, control (SH-WT) and knock-out for NPC1 (SH-NPC), were treated with increasing concentration of MPP^+. A) MTT reduction was accessed 24 h after treatment with 0.5, 1 and 2 mM MPP^+. Results represent mean values ± SEM of at least ten independent experiments performed in triplicates and are expressed as a percentage of MTT reduction relative to the correspondent vehicle-treated cells. B) LDH released from cells was determined with the CytoTox96® Non-Radioactive Cytotoxicity Assay kit 72 h after treatment with 0.5, 1 and 2 mM MPP^+. Results represent mean values ± SEM of at least five independent experiments performed in triplicates and are expressed as a percentage of LDH release in lysed cells. Statistical analysis was performed by Kruskal Wallis followed by Dunn's multiple comparisons test, for the MTT reduction assay, and by one-way ANOVA followed by Dunnett's multiple comparisons test, for the LDH release assay (*$p < 0.05$, **$p < 0.01$, ***$p < 0.001$).

transcripts when compared with vehicle-treated controls (Fig. 9A). *Npc1* mRNA levels decreased 55 % 6 h after MPTP treatment, while *Ldlr* decreased about 50 % and *Lipa* about 30 % in the same samples. In the striatum we observed a similar profile, with significant decreases in the mRNA levels of *Apoe* and *Npc1* 6 h after MPTP treatment, while *Lipa* mRNA levels were already significantly decreased at 3 h, and further reduced to 65 % of control values 6 h after MPTP administration (Fig. 9A).

Thus, in the nigro-striatal pathway of mouse brain MPTP administration recapitulates the mRNA changes seen in N2a cells after MPP^+ treatment, namely a decrease in the expression of genes involved in cholesterol-internalization and lysosomal content such as *Ldlr*, *Npc1* and *Lipa*. Such changes further suggest that mitochondrial dysfunction could lead to an impairment in cholesterol distribution *via* late endosomal/lysosomal pathway.

To further confirm these results, and to determine if the previously

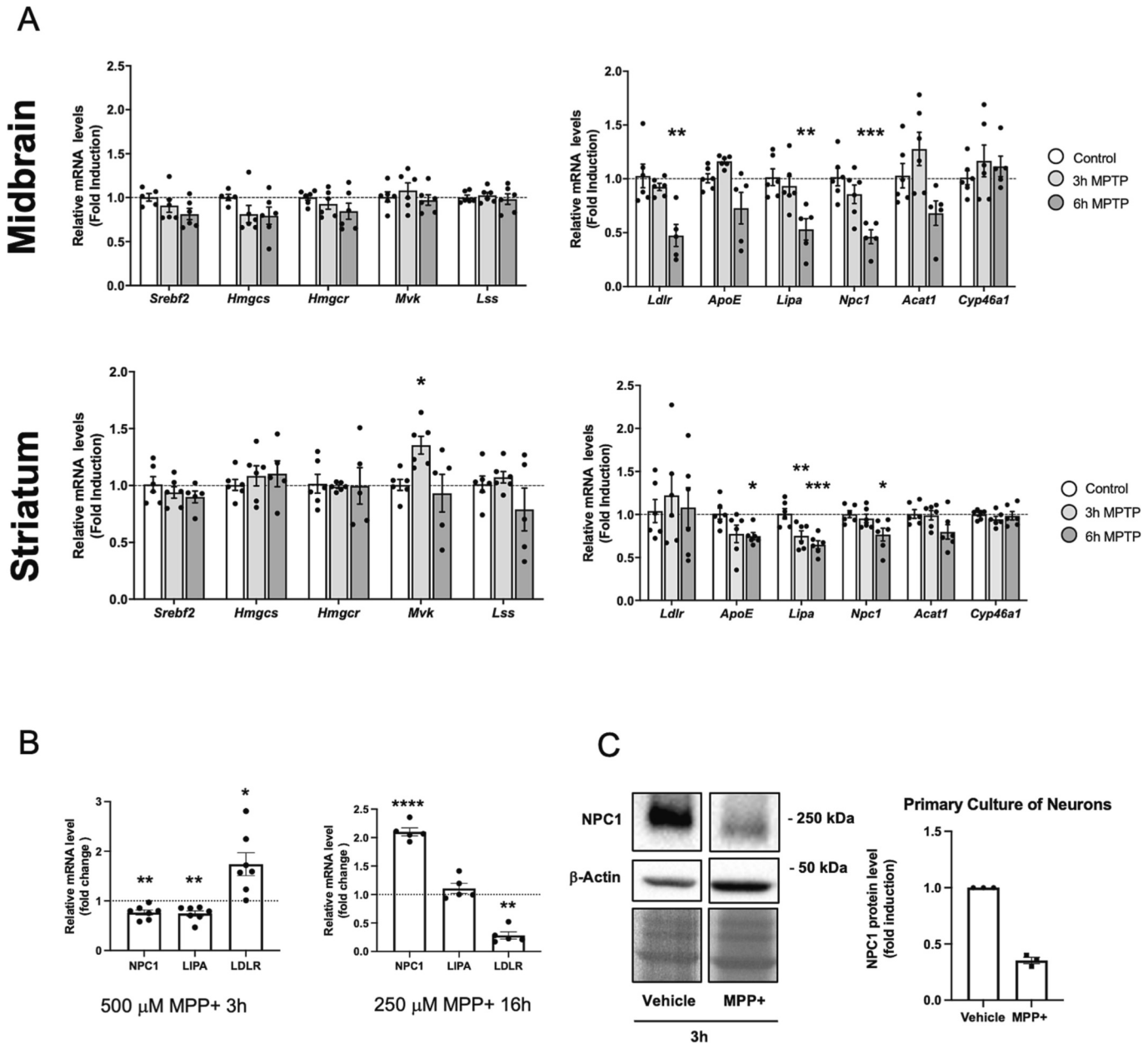

Fig. 9. NPC1 mRNA levels are downregulated in the midbrain and striatum of MPTP-treated mice. A) RT-qPCR analysis of the mRNA levels of genes involved in biosynthesis (*Srebf2*, *Hmgcs*, *Hmgcr, Mvk and Lss*), efflux (*ApoE* and *Cyp46a1*), uptake (*Ldlr*), storage (*Acat1* and *Lipa*) and intracellular cholesterol transport (*Npc1*). Mice were treated with a single i.p. injection of 40 mg/kg of MPTP or saline and sacrificed after 3 or 6 h. Normalization was achieved using the internal standard Eef. Data is represented as mean values ± SEM from at least five animals per condition, and each sample was assayed in duplicate. Statistical analysis was performed by one-way ANOVA followed by Dunnett's multiple comparisons test (*$p < 0.05$, **$p < 0.01$, ***$p < 0.001$). B) RT-qPCR analysis of *Npc1*, *Lipa*, and *Ldlr* mRNA levels, in primary cultures of mouse cortical neurons 15 days *in vitro*. Neurons were treated for 3 h with 500 µM MPP^+, or for 16 h with 250 µM MPP^+. Values were normalized using the internal standard Eef. Data is represented as mean values ± SEM from at least five individual experiments, performed with two technical replicates and is expressed as fold change over control. Statistical analysis was performed by one-way ANOVA followed by Dunnett's multiple comparisons test (*$p < 0.05$; **$p < 0.01$; ***$p < 0.001$ *vs* vehicle treated cells). C) Western Blot analysis of NPC1 protein levels in primary cultures of mouse cortical neurons 15 days *in vitro* treated for 3 h with 500 µM MPP^+. Left panel show representative immunoblots for NPC1, and β-actin which was used as loading control, and Amido Black staining. Results are shown as fold induction over vehicle treated cells and are expressed as mean values ± SEM of at least three different experiments. Statistical analysis was performed using Student's *t*-test.

described changes can be due to gene expression changes that occur in neurons, we evaluated the *Npc1* mRNA and protein levels in primary cultures of mice cortical neurons, and the transcript levels of genes that were shown to be downregulated in the midbrain of MPTP-treated mice, such as *Lipa* and *Ldlr*. In agreement with our *in vivo* results, treatment with 500 μM MPP^+ led to an early significant decrease of *Npc*1 transcripts and protein levels 3 h following MPP^+ treatment (Fig. 9B and C). This agrees with previous results that show that the effect of MPP^+ in primary cultures of mice neurons is faster and more striking in comparison with neuroblastoma cells, since neurons largely depend on oxidative phosphorylation. Due to this fact, for the analysis of MPP^+ effect at later time points, we are obliged to treat cells with 250 μM MPP^+, since higher concentrations induced substantial cell death. Interestingly, after an initial downregulation, *Npc1* levels are increased 2-fold 16 h after MPP^+ treatment. Similarly, *Lipa* expression levels are downregulated by MPP^+ treatment at an early time-point, while no changes are detected at the later time point. Surprisingly, *Ldlr* expression shows an opposite response to MPP^+ *in vitro*.

3.7. NPC1 protein levels are inversely correlated with Braak stage in PD patients

To further corroborate our results, we obtained Human brain samples from the Netherlands Brain Bank. Mesencephalon tissue samples of 4 PD patients (age range: 68–79; m/f: 3/1) and 4 control subjects (age range: 77–92; m/f; 2/2), were selected based on clinical diagnosis confirmed by neuropathological evaluation. Controls had no known clinical history of dementia or motor disturbance and the cause of death was unrelated to the CNS. We started by evaluating by Western blot analysis the protein expression level of NPC1 in total protein extracts isolated from the human tissue samples (Fig. 10A). Our results shown a high variability in NPC1 expression levels both in controls and PD patients, and no significant differences were observed. Nevertheless, when we correlated NPC1 protein levels normalized to β-actin, with age and Braak stage in PD patients and controls, we observed a significant negative correlation between NPC1 protein levels and Braak stage, showing that as disease progresses, there is a concomitant

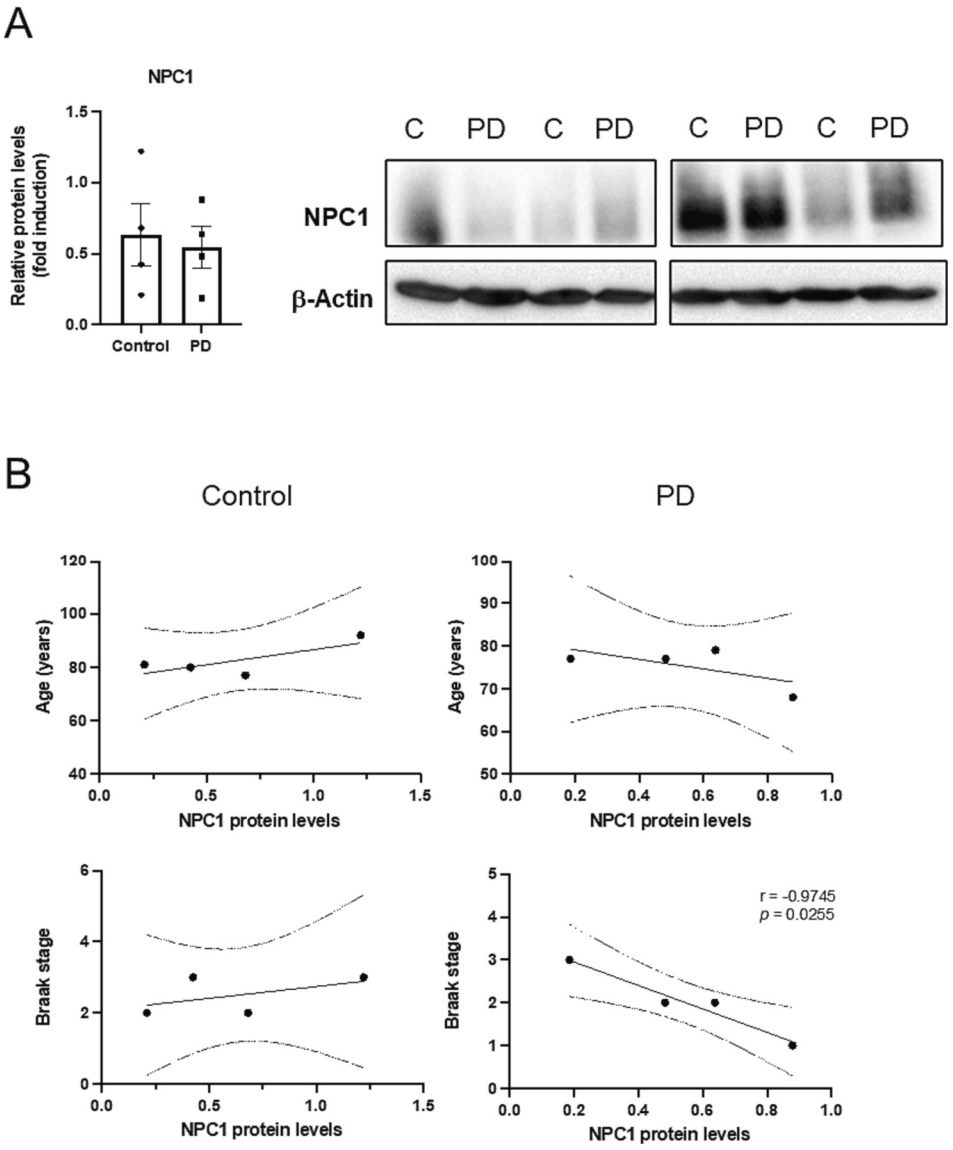

Fig. 10. NPC1 protein levels decrease as Braak stage increases in PD patients. A) NPC1 protein levels were determined in 4 PD patients (PD) and 4 age-matched controls (C) by Western blot analysis. In the right panel the immunoblots of NPC1 and the loading control, β-actin is shown. Results are plotted in the right panel as fold induction over the mean values of NPC1 levels found in controls ± SEM. Statistical analysis was performed using Student's *t*-test. B) Correlation between NPC1 protein levels normalized to β-actin, age and Braak stage in PD patients and controls. Each point represents a separate case. The best-fit linear regression (solid lines) and 95 % confidence intervals (interrupted lines) are superimposed. Only significant *p*-values (and associated Pearson correlation coefficient r) are shown.

downregulation of NPC1 (Fig. 10B).

4. Discussion

In recent years, there has been a growing body of research indicating that lysosomal dysfunction plays a vital role in PD, as evidenced by genetic, biochemical, and cellular pathway studies [17]. Indeed, variants in the *GBA* gene, which encodes for glucocerebrosidase, are established as the most common risk factors for PD [47]. Patients harboring a GBA mutation exhibit an earlier disease onset, a higher likelihood of affected relatives, and an increased tendency for atypical clinical manifestations. Additionally, approximately 56 % of Parkinson's disease patients carry at least one potentially deleterious variant in a lysosomal storage disorder gene, while 21 % carry multiple alleles [48].

Herein, we show that MPP^+-induced mitochondrial dysfunction leads to an NPC1-like phenotype, characterized by the accumulation of unesterified cholesterol within lysosomes. Interestingly, parkinsonian syndrome has been described in NPC1 heterozygotes [49,50], while in *in vitro* models of heterozygous and homozygous GBA1 mutations, lysosomal dysfunction was accompanied by increased intracellular cholesterol levels when compared to wild type GBA1 cells [51].

By quantifying the levels of total, free and esterified cholesterol, we show that N2a neuroblastoma cells have increased cholesterol levels as an early response to a high dose of MPP^+ treatment. Moreover, this outcome seems to be exclusive to the parkinsonism-inducing toxin since other drugs that target mitochondrial function did not induce a similar response. In agreement, MPP^+ specifically reduced NPC1 mRNA levels, when compared to the mitochondrial uncoupler CCCP and to other mitochondrial toxins (*i.e.*, antimycin-A that targets complex III, and oligomycin that targets ATP synthase). The decrease in NPC1, both at the mRNA and protein levels, is also observed in primary cultures of mouse neurons treated with MPP^+.

The interdependence of cholesterol accumulation and lysosomal dysfunction has been well acknowledged in Niemann-Pick type C disease [52], but this has been hardly addressed in other neurodegenerative disorders, although accumulation of cholesterol in lysosomes has been associated with defective autophagy. In this case, the maturation of autophagosomes is impaired because of defective amphisome formation caused by failure in SNARE machinery [53].

In parallel with the MPP^+-induced accumulation of unesterified cholesterol within lysosomes we observed a decrease in the expression and transcriptional activity of SREBP2, and in its downstream targets, *Hmgcs* and *Hmgcr*. Thus, our data suggest that drug-induced mitochondrial insult leads to intracellular cholesterol accumulation and consequently to a decrease in SREBP transcriptional activity and a downregulation of genes involved in cholesterol synthesis. Since the decreased expression of cholesterogenic genes was observed with all the mitochondrial toxins tested, the inhibition of cholesterol synthesis is most likely a common response to mitochondrial oxidative damage, and to the decrease in ATP levels. Interestingly, Wall and colleagues, demonstrated that in human fibroblasts, inhibiting the mitochondrial respiratory chain results in a decrease in intracellular levels of sterol intermediates involved in cholesterol biosynthesis [54]. This research also highlights the impact of rotenone and oligomycin A on various metabolites within the cholesterol synthesis pathway, with distinct effects on different parts of the pathway. For instance, while antimycin A, but not rotenone, significantly reduced the precursors of sterol synthesis, namely squalene and oxidosqualene, all three mitochondrial inhibitors — rotenone, antimycin A, and oligomycin A — showed a significant reduction in lanosterol, the initial metabolite dedicated to cholesterol synthesis. Furthermore, downstream sterol metabolites such as zymosterol, zymostenol, lathosterol, and desmosterol were consistently diminished when the respiratory chain was inhibited, regardless of the specific complex affected. Notably, despite the decrease in these intermediates, rotenone-induced inhibition led to an elevation in the intracellular free cholesterol pool, aligned with our own research findings, and suggesting that the effect of MPP+ is probably because of complex I inhibition.

Moreover, not all mitochondrial insults affected the endosomal/lysosomal pathway equally, since there was a specific repression of *Npc1* and of markers of lysosomal biogenesis after treatment with MPP^+. Interestingly, our results show decreased *Tfeb* expression after MPP^+ treatment. TFEB is a transcription factor that remains in close association with lysosomal membranes due to phosphorylation by mTORC1. However, during situations of energy depletion, AMPK supresses mTORC1 activity resulting in its release. This allows TFEB to reach the nucleus, stimulating the expression of various proteins involved in lysosomal function [55,56].

There is extensive evidence of AMPK activation under stressful conditions like oxidative stress [57–59]. For instance, in SH-SY5Y cells treated with 2 mM MPP^+ there is an increase in p-AMPK levels as soon as 2 h after treatment, and this activation could be prevented by pre-treatment with the antioxidants *N*-acetylcysteine and butylated hydroxyanisole [42]. It is also well documented that under acute mitochondrial stress, AMPK is activated which results in mTORC1 inhibition [36]. In agreement, our results show an early and transient activation of AMPK together with decreased ATP levels. Interestingly, we observed that at the same time-point there is an increase in mTOR phosphorylation. These findings contradict prior studies that suggested that the pharmacologically-induced impairment of mitochondrial function leads to mTORC1 inhibition, primarily attributed to AMPK activation resulting from decreased energy levels [60]. Contrary, and in agreement with our results, it has been described that in mitochondrially defective neurons, ribosomal S6 and S6 kinase phosphorylation increase over time, despite activation of AMPK [61]. Understanding this paradoxical simultaneous activation of AMPK and mTORC1 at 6 h of MPP^+ treatment requires further studies. Nonetheless, in NPC disease it has been reported that loss of NPC1 function leads to mTORC1 hyperactivation [39].

The increase in lysosomal cholesterol levels and the concomitant increase in mTOR phosphorylation induced by MPP^+ can explain the differential effect of MPP^+ and CCCP on the activation of autophagy. Indeed, we and others have shown that in neuronal cells, CCCP treatment induces the lipidation of LC3II as early as 3 h after treatment [62], while autophagy activation is delayed after complex I inhibition [9,63]. Autophagy can have both positive and unfavorable consequences, and excessive or prolonged activation of autophagy can lead to the degradation of functional mitochondria, which could exacerbate mitochondrial dysfunction and contribute to neurodegeneration. Indeed, it is possible that the accumulation of cholesterol within the cell, which is observed following treatment with MPP^+, is a protective cellular mechanism activated in response to mitochondrial damage, that may delay the activation of signaling pathways that would otherwise trigger the induction of cell death. In agreement we observed that cells knockout for NPC1 are more resistant to MPP^+-induced cell death compared with cells that express this protein.

Mitochondrial dysfunction may be reversible and delaying autophagy activation could give the cell time to repair the mitochondrial damage, rather than disposing of it. Indeed, mitochondria can still function to some extent even when complex I is inhibited, and alternative pathways can counterweigh for the loss of complex I activity. For example, complex II (succinate dehydrogenase) can provide electrons to the electron transport chain, downstream of complex I, bypassing the need for complex I activity [64]. Notably, a comprehensive analysis of mitochondrial respiration in neuronal cells following MPP+ treatment revealed that before complex I inhibition, there is an augmentation of complex II activity, indicating the existence of a compensatory mechanism [65]. Additionally, alternative electron carriers, such as the glycerol-3-phosphate shuttle and the electron-transferring flavoprotein system, can also contribute to electron transport and maintain mitochondrial function in the absence of complex I activity [66]. Delaying the activation of autophagy could also give the cell time to mount a

proper stress response to the mitochondrial dysfunction. Interestingly, the functionality of mitochondrial complex I has emerged as a significant contributor to the initiation, extent, and duration of the autophagic response. Remarkably, phenformin treatment or genetic impairments in complex I have demonstrated the ability to inhibit autophagy induced by mTOR inhibitors, while approaches that enhance mitochondrial metabolism have shown to augment autophagy [67]. The search for autophagy inhibitors through phenotypic screening yielded the identification of aumitin, a novel compound with potent autophagy inhibitory properties [68]. Following target identification and validation, it was determined that aumitin exerts its inhibitory effect on mitochondrial respiration by specifically targeting complex I.

In agreement with our *in vitro* data, MPTP administration recapitulates in the nigro-striatal pathway of mouse brain, the decreased expression of genes involved in cholesterol uptake and lysosomal content such as *Ldlr*, *Npc1* and *Lipa*. Conversely, we did not observe alterations in the levels of total cholesterol (data not shown). This is not surprising, since transient cholesterol accumulation would be difficult to detect, due to bulk myelin cholesterol. Additionally, the analysis of NPC1 levels in human PD brain samples, suggests that the levels of this protein progressively decrease with the disease course, which confirms our previous results in different *in vitro* and *in vivo* models, and highlights NPC1 as a player in the pathogenesis of PD. Interestingly, NPC1 mRNA and protein levels were also shown to be affected in Alzheimer's disease (AD) brain samples, however an up-regulation was detected in the hippocampus and frontal cortex of AD when compared to the controls [69].

In summary, we demonstrate that in neuronal cells, inhibition of mitochondrial complex I by MPP^+ leads to reduced NPC1 expression, intracellular cholesterol accumulation and altered mTOR signaling, and that the knock-out of NPC1 protects cells against cell death induced by acute mitochondrial damage. Thus, NPC1 should also be considered a potential disease-modifying target in PD.

Supplementary data to this article can be found online at https://doi.org/10.1016/j.bbadis.2023.166980.

Funding

The work was supported by FEDER/Programa Operacional Regional de Lisboa – Lisboa 2020 (LISBOA-01-0145-FEDER-030104) and by National funds from Fundação para a Ciência e a Tecnologia (PTDC/MEDFSL/30104/2017), and by the Swedish Research Council.

CRediT authorship contribution statement

Inês Caria: Validation, Formal analysis, Investigation, Visualization, Writing – original draft, Writing – review & editing. **Maria João Nunes:** Conceptualization, Validation, Formal analysis, Investigation, Visualization, Supervision, Writing – review & editing. **Viviana Ciraci:** Validation, Formal analysis, Investigation, Writing – review & editing. **Andreia Neves Carvalho:** Validation, Investigation, Supervision, Writing – review & editing. **Catarina Ranito:** Investigation, Writing – review & editing. **Susana G. Santos:** Investigation, Writing – review & editing. **Maria João Gama:** Conceptualization, Resources, Supervision, Writing – review & editing. **Margarida Castro-Caldas:** Conceptualization, Validation, Supervision, Resources, Writing – review & editing. **Cecília M.P. Rodrigues:** Resources, Supervision, Writing – review & editing. **Jorge L. Ruas:** Conceptualization, Resources, Project administration, Funding acquisition, Writing – review & editing. **Elsa Rodrigues:** Conceptualization, Validation, Formal analysis, Investigation, Resources, Writing – original draft, Writing – review & editing, Visualization, Supervision, Project administration, Funding acquisition.

Declaration of competing interest

The authors declare that they have no known competing financial interests or personal relationships that could have appeared to influence the work reported in this paper.

Data availability

Data will be made available on request.

References

[1] D. Li, J. Zhang, Q. Liu, Brain cell type-specific cholesterol metabolism and implications for learning and memory, Trends Neurosci. 45 (2022) 401–414.
[2] W. Poewe, K. Seppi, C.M. Tanner, G.M. Halliday, P. Brundin, J. Volkmann, A. E. Schrag, A.E. Lang, Parkinson disease, Nat. Rev. Dis. Primers. 3 (2017) 17013.
[3] P.M. Keeney, J. Xie, R.A. Capaldi, J.P. Bennett Jr., Parkinson's disease brain mitochondrial complex I has oxidatively damaged subunits and is functionally impaired and misassembled, J. Neurosci. 26 (2006) 5256–5264.
[4] S.R. Subramaniam, M.F. Chesselet, Mitochondrial dysfunction and oxidative stress in Parkinson's disease, Prog. Neurobiol. 106-107 (2013) 17–32.
[5] G.E. Meredith, D.J. Rademacher, MPTP mouse models of Parkinson's disease: an update, J. Parkinsons Dis. 1 (2011) 19–33.
[6] A.N. Carvalho, C. Marques, E. Rodrigues, C.J. Henderson, C.R. Wolf, P. Pereira, M. J. Gama, Ubiquitin-proteasome system impairment and MPTP-induced oxidative stress in the brain of C57BL/6 wild-type and GSTP knockout mice, Mol. Neurobiol. 47 (2013) 662–672.
[7] M. Castro-Caldas, A.N. Carvalho, E. Rodrigues, C.J. Henderson, C.R. Wolf, C. M. Rodrigues, M.J. Gama, Tauroursodeoxycholic acid prevents MPTP-induced dopaminergic cell death in a mouse model of Parkinson's disease, Mol. Neurobiol. 46 (2012) 475–486.
[8] M.O. Mendes, A.I. Rosa, A.N. Carvalho, M.J. Nunes, P. Dionisio, E. Rodrigues, D. Costa, S. Duarte-Silva, P. Maciel, C.M.P. Rodrigues, M.J. Gama, M. Castro-Caldas, Neurotoxic effects of MPTP on mouse cerebral cortex: modulation of neuroinflammation as a neuroprotective strategy, Mol. Cell. Neurosci. 96 (2019) 1–9.
[9] A.I. Rosa, I. Fonseca, M.J. Nunes, S. Moreira, E. Rodrigues, A.N. Carvalho, C.M. P. Rodrigues, M.J. Gama, M. Castro-Caldas, Novel insights into the antioxidant role of tauroursodeoxycholic acid in experimental models of Parkinson's disease, Biochim. Biophys. Acta Mol. Basis Dis. 2017 (1863) 2171–2181.
[10] S. Torres, C.M. Garcia-Ruiz, J.C. Fernandez-Checa, Mitochondrial cholesterol in Alzheimer's disease and Niemann-pick type C disease, Front. Neurol. 10 (2019) 1168.
[11] C.B. Do, J.Y. Tung, E. Dorfman, A.K. Kiefer, E.M. Drabant, U. Francke, J. L. Mountain, S.M. Goldman, C.M. Tanner, J.W. Langston, A. Wojcicki, N. Eriksson, Web-based genome-wide association study identifies two novel loci and a substantial genetic component for Parkinson's disease, PLoS Genet. 7 (2011), e1002141.
[12] R.M. Ivatt, A.J. Whitworth, SREBF1 links lipogenesis to mitophagy and sporadic Parkinson disease, Autophagy 10 (2014) 1476–1477.
[13] E.M. Toledo, S. Yang, D. Gyllborg, K.E. van Wijk, I. Sinha, M. Varas-Godoy, C. L. Grigsby, P. Lonnerberg, S. Islam, K.R. Steffensen, S. Linnarsson, E. Arenas, Srebf1 controls midbrain dopaminergic neurogenesis, Cell Rep. 31 (2020), 107601.
[14] R. Musanti, E. Parati, E. Lamperti, G. Ghiselli, Decreased cholesterol biosynthesis in fibroblasts from patients with Parkinson disease, Biochem. Med. Metab. Biol. 49 (1993) 133–142.
[15] K.Y. Kim, M.V. Stevens, M.H. Akter, S.E. Rusk, R.J. Huang, A. Cohen, A. Noguchi, D. Springer, A.V. Bocharov, T.L. Eggerman, D.F. Suen, R.J. Youle, M. Amar, A. T. Remaley, M.N. Sack, Parkin is a lipid-responsive regulator of fat uptake in mice and mutant human cells, J. Clin. Invest. 121 (2011) 3701–3712.
[16] H.J.R. Fernandes, N. Patikas, S. Foskolou, S.F. Field, J.E. Park, M.L. Byrne, A. R. Bassett, E. Metzakopian, Single-cell transcriptomics of Parkinson's disease human in vitro models reveals dopamine neuron-specific stress responses, Cell Rep. 33 (2020), 108263.
[17] A.D. Klein, J.R. Mazzulli, Is Parkinson's disease a lysosomal disorder? Brain J. Neurol. 141 (2018) 2255–2262.
[18] M. Moutinho, M.J. Nunes, E. Rodrigues, Cholesterol 24-hydroxylase: brain cholesterol metabolism and beyond, Biochim. Biophys. Acta 2016 (1861) 1911–1920.
[19] C.L. Andersen, J.L. Jensen, T.F. Orntoft, Normalization of real-time quantitative reverse transcription-PCR data: a model-based variance estimation approach to identify genes suited for normalization, applied to bladder and colon cancer data sets, Cancer Res. 64 (2004) 5245–5250.
[20] S. Moreira, I. Fonseca, M.J. Nunes, A. Rosa, L. Lemos, E. Rodrigues, A.N. Carvalho, T.F. Outeiro, C.M.P. Rodrigues, M.J. Gama, M. Castro-Caldas, Nrf2 activation by tauroursodeoxycholic acid in experimental models of Parkinson's disease, Exp. Neurol. 295 (2017) 77–87.
[21] S.S. Thomas, Y.S. Cha, K.A. Kim, Effect of vegetable oils with different fatty acid composition on high-fat diet-induced obesity and colon inflammation, Nutr. Res. Pract. 14 (2020) 425–437.
[22] P.M. Rodrigues, M.B. Afonso, A.L. Simao, C.C. Carvalho, A. Trindade, A. Duarte, P. M. Borralho, M.V. Machado, H. Cortez-Pinto, C.M. Rodrigues, R.E. Castro, miR-21 ablation and obeticholic acid ameliorate nonalcoholic steatohepatitis in mice, Cell Death Dis. 8 (2017), e2748.

[23] J.A. Yoon, D.H. Han, J.Y. Noh, M.H. Kim, G.H. Son, K. Kim, C.J. Kim, Y.K. Pak, S. Cho, Meal time shift disturbs circadian rhythmicity along with metabolic and behavioral alterations in mice, PloS One 7 (2012), e44053.
[24] I.C. Ferder, L. Fung, Y. Ohguchi, X. Zhang, K.G. Lassen, D. Capen, D. Brown, R. J. Xavier, N. Wang, Meiotic gatekeeper STRA8 suppresses autophagy by repressing Nr1d1 expression during spermatogenesis in mice, PLoS Genet. 15 (2019), e1008084.
[25] D. Cirera-Salinas, M. Pauta, R.M. Allen, A.G. Salerno, C.M. Ramirez, A. Chamorro-Jorganes, A.C. Wanschel, M.A. Lasuncion, M. Morales-Ruiz, Y. Suarez, A. Baldan, E. Esplugues, C. Fernandez-Hernando, Mir-33 regulates cell proliferation and cell cycle progression, Cell Cycle 11 (2012) 922–933.
[26] A.B. Castoreno, Y. Wang, W. Stockinger, L.A. Jarzylo, H. Du, J.C. Pagnon, E. C. Shieh, A. Nohturfft, Transcriptional regulation of phagocytosis-induced membrane biogenesis by sterol regulatory element binding proteins, Proc. Natl. Acad. Sci. U. S. A. 102 (2005) 13129–13134.
[27] I. Milagre, M.J. Nunes, M.J. Gama, R.F. Silva, J.M. Pascussi, M.C. Lechner, E. Rodrigues, Transcriptional regulation of the human CYP46A1 brain-specific expression by Sp transcription factors, J. Neurochem. 106 (2008) 835–849.
[28] M. Moutinho, M.J. Nunes, A.Q. Gomes, M.J. Gama, A. Cedazo-Minguez, C. M. Rodrigues, I. Bjorkhem, E. Rodrigues, Cholesterol 24S-hydroxylase overexpression inhibits the liver X receptor (LXR) pathway by activating small guanosine triphosphate-binding proteins (sGTPases) in neuronal cells, Mol. Neurobiol. 51 (2015) 1489–1503.
[29] J. Bove, C. Perier, Neurotoxin-based models of Parkinson's disease, Neuroscience 211 (2012) 51–76.
[30] J. Zhu, R.K. Dagda, C.T. Chu, Monitoring mitophagy in neuronal cell cultures, Methods Mol. Biol. 793 (2011) 325–339.
[31] W.A. Cramer, S.S. Hasan, E. Yamashita, The Q cycle of cytochrome bc complexes: a structure perspective, Biochim. Biophys. Acta 2011 (1807) 788–802.
[32] J. Symersky, D. Osowski, D.E. Walters, D.M. Mueller, Oligomycin frames a common drug-binding site in the ATP synthase, Proc. Natl. Acad. Sci. U. S. A. 109 (2012) 13961–13965.
[33] M.T. Vanier, Niemann-pick disease type C, Orphanet J. Rare Dis. 5 (2010) 16.
[34] F.R. Maxfield, D. Wustner, Analysis of cholesterol trafficking with fluorescent probes, Methods Cell Biol. 108 (2012) 367–393.
[35] L. Fernandez-Mosquera, C.V. Diogo, K.F. Yambire, G.L. Santos, M. Luna Sanchez, P. Benit, P. Rustin, L.C. Lopez, I. Milosevic, N. Raimundo, Acute and chronic mitochondrial respiratory chain deficiency differentially regulate lysosomal biogenesis, Sci. Rep. 7 (2017) 45076.
[36] D. Garcia, R.J. Shaw, AMPK: mechanisms of cellular energy sensing and restoration of metabolic balance, Mol. Cell 66 (2017) 789–800.
[37] P.R. Clarke, D.G. Hardie, Regulation of HMG-CoA reductase: identification of the site phosphorylated by the AMP-activated protein kinase in vitro and in intact rat liver, EMBO J. 9 (1990) 2439–2446.
[38] Y. Li, S. Xu, M.M. Mihaylova, B. Zheng, X. Hou, B. Jiang, O. Park, Z. Luo, E. Lefai, J. Y. Shyy, B. Gao, M. Wierzbicki, T.J. Verbeuren, R.J. Shaw, R.A. Cohen, M. Zang, AMPK phosphorylates and inhibits SREBP activity to attenuate hepatic steatosis and atherosclerosis in diet-induced insulin-resistant mice, Cell Metab. 13 (2011) 376–388.
[39] O.B. Davis, H.R. Shin, C.Y. Lim, E.Y. Wu, M. Kukurugya, C.F. Maher, R.M. Perera, M.P. Ordonez, R. Zoncu, NPC1-mTORC1 signaling couples cholesterol sensing to organelle homeostasis and is a targetable pathway in Niemann-Pick type C, Dev. Cell 56 (2021) 260–276 e267.
[40] J.S. Choi, C. Park, J.W. Jeong, AMP-activated protein kinase is activated in Parkinson's disease models mediated by 1-methyl-4-phenyl-1,2,3,6-tetrahydropyridine, Biochem. Biophys. Res. Commun. 391 (2010) 147–151.
[41] B. Dehay, J. Bove, N. Rodriguez-Muela, C. Perier, A. Recasens, P. Boya, M. Vila, Pathogenic lysosomal depletion in Parkinson's disease, J. Neurosci. 30 (2010) 12535–12544.
[42] M. Jovanovic-Tucovic, L. Harhaji-Trajkovic, M. Dulovic, G. Tovilovic-Kovacevic, N. Zogovic, M. Jeremic, M. Mandic, V. Kostic, V. Trajkovic, I. Markovic, AMP-activated protein kinase inhibits MPP+-induced oxidative stress and apoptotic death of SH-SY5Y cells through sequential stimulation of Akt and autophagy, Eur. J. Pharmacol. 863 (2019), 172677.
[43] D.M. Arduino, A.R. Esteves, L. Cortes, D.F. Silva, B. Patel, M. Grazina, R. H. Swerdlow, C.R. Oliveira, S.M. Cardoso, Mitochondrial metabolism in Parkinson's disease impairs quality control autophagy by hampering microtubule-dependent traffic, Hum. Mol. Genet. 21 (2012) 4680–4702.
[44] S. Sakamoto, M. Miyara, S. Sanoh, S. Ohta, Y. Kotake, Mild MPP(+) exposure-induced glucose starvation enhances autophagosome synthesis and impairs its degradation, Sci. Rep. 7 (2017) 46668.
[45] J.D. Horton, J.L. Goldstein, M.S. Brown, SREBPs: activators of the complete program of cholesterol and fatty acid synthesis in the liver, J. Clin. Invest. 109 (2002) 1125–1131.
[46] M.S. Saporito, B.A. Thomas, R.W. Scott, MPTP activates c-Jun NH(2)-terminal kinase (JNK) and its upstream regulatory kinase MKK4 in nigrostriatal neurons in vivo, J. Neurochem. 75 (2000) 1200–1208.
[47] E. Sidransky, M.A. Nalls, J.O. Aasly, J. Aharon-Peretz, G. Annesi, E.R. Barbosa, A. Bar-Shira, D. Berg, J. Bras, A. Brice, C.M. Chen, L.N. Clark, C. Condroyer, E.V. De Marco, A. Durr, M.J. Eblan, S. Fahn, M.J. Farrer, H.C. Fung, Z. Gan-Or, T. Gasser, R. Gershoni-Baruch, N. Giladi, A. Griffith, T. Gurevich, C. Januario, P. Kropp, A. E. Lang, G.J. Lee-Chen, S. Lesage, K. Marder, I.F. Mata, A. Mirelman, J. Mitsui, I. Mizuta, G. Nicoletti, C. Oliveira, R. Ottman, A. Orr-Urtreger, L.V. Pereira, A. Quattrone, E. Rogaeva, A. Rolfs, H. Rosenbaum, R. Rozenberg, A. Samii, T. Samaddar, C. Schulte, M. Sharma, A. Singleton, M. Spitz, E.K. Tan, N. Tayebi, T. Toda, A.R. Troiano, S. Tsuji, M. Wittstock, T.G. Wolfsberg, Y.R. Wu, C. P. Zabetian, Y. Zhao, S.G. Ziegler, Multicenter analysis of glucocerebrosidase mutations in Parkinson's disease, N. Engl. J. Med. 361 (2009) 1651–1661.
[48] L.A. Robak, I.E. Jansen, J. van Rooij, A.G. Uitterlinden, R. Kraaij, J. Jankovic, C. International Parkinson's Disease Genomics, P. Heutink, J.M. Shulman, Excessive burden of lysosomal storage disorder gene variants in Parkinson's disease, Brain 140 (2017) 3191–3203.
[49] K.A. Josephs, J.Y. Matsumoto, N.M. Lindor, Heterozygous Niemann-pick disease type C presenting with tremor, Neurology 63 (2004) 2189–2190.
[50] H.H. Kluenemann, J.G. Nutt, M.Y. Davis, T.D. Bird, Parkinsonism syndrome in heterozygotes for Niemann-pick C1, J. Neurol. Sci. 335 (2013) 219–220.
[51] J. Magalhaes, M.E. Gegg, A. Migdalska-Richards, M.K. Doherty, P.D. Whitfield, A. H. Schapira, Autophagic lysosome reformation dysfunction in glucocerebrosidase deficient cells: relevance to Parkinson disease, Hum. Mol. Genet. 25 (2016) 3432–3445.
[52] K. Sobo, I. Le Blanc, P.P. Luyet, M. Fivaz, C. Ferguson, R.G. Parton, J. Gruenberg, F. G. van der Goot, Late endosomal cholesterol accumulation leads to impaired intra-endosomal trafficking, PloS One 2 (2007), e851.
[53] S. Sarkar, B. Carroll, Y. Buganim, D. Maetzel, A.H. Ng, J.P. Cassady, M.A. Cohen, S. Chakraborty, H. Wang, E. Spooner, H. Ploegh, J. Gsponer, V.I. Korolchuk, R. Jaenisch, Impaired autophagy in the lipid-storage disorder Niemann-Pick type C1 disease, Cell Rep. 5 (2013) 1302–1315.
[54] C.T.J. Wall, G. Lefebvre, S. Metairon, P. Descombes, A. Wiederkehr, J. Santo-Domingo, Mitochondrial respiratory chain dysfunction alters ER sterol sensing and mevalonate pathway activity, J. Biol. Chem. 298 (2022), 101652.
[55] A. Roczniak-Ferguson, C.S. Petit, F. Froehlich, S. Qian, J. Ky, B. Angarola, T. C. Walther, S.M. Ferguson, The transcription factor TFEB links mTORC1 signaling to transcriptional control of lysosome homeostasis, Sci. Signal. 5 (2012) ra42.
[56] C. Settembre, R. Zoncu, D.L. Medina, F. Vetrini, S. Erdin, S. Erdin, T. Huynh, M. Ferron, G. Karsenty, M.C. Vellard, V. Facchinetti, D.M. Sabatini, A. Ballabio, A lysosome-to-nucleus signalling mechanism senses and regulates the lysosome via mTOR and TFEB, EMBO J. 31 (2012) 1095–1108.
[57] D.G. Hardie, AMPK–sensing energy while talking to other signaling pathways, Cell Metab. 20 (2014) 939–952.
[58] R.C. Rabinovitch, B. Samborska, B. Faubert, E.H. Ma, S.P. Gravel, S. Andrzejewski, T.C. Raissi, A. Pause, J. St-Pierre, R.G. Jones, AMPK maintains cellular metabolic homeostasis through regulation of mitochondrial reactive oxygen species, Cell Rep. 21 (2017) 1–9.
[59] T. Sanli, G.R. Steinberg, G. Singh, T. Tsakiridis, AMP-activated protein kinase (AMPK) beyond metabolism: a novel genomic stress sensor participating in the DNA damage response pathway, Cancer Biol. Ther. 15 (2014) 156–169.
[60] R. Zoncu, A. Efeyan, D.M. Sabatini, mTOR: from growth signal integration to cancer, diabetes and ageing, Nat. Rev. Mol. Cell Biol. 12 (2011) 21–35.
[61] X. Zheng, L. Boyer, M. Jin, Y. Kim, W. Fan, C. Bardy, T. Berggren, R.M. Evans, F. H. Gage, T. Hunter, Alleviation of neuronal energy deficiency by mTOR inhibition as a treatment for mitochondria-related neurodegeneration, Elife 5 (2016).
[62] I. Fonseca, G. Gordino, S. Moreira, M.J. Nunes, C. Azevedo, M.J. Gama, E. Rodrigues, C.M.P. Rodrigues, M. Castro-Caldas, Tauroursodeoxycholic acid protects against mitochondrial dysfunction and cell death via mitophagy in human neuroblastoma cells, Mol. Neurobiol. 54 (2017) 6107–6119.
[63] J. Lim, H.W. Kim, M.B. Youdim, I.J. Rhyu, K.M. Choe, Y.J. Oh, Binding preference of p62 towards LC3-ll during dopaminergic neurotoxin-induced impairment of autophagic flux, Autophagy 7 (2011) 51–60.
[64] N. Esteitie, R. Hinttala, R. Wibom, H. Nilsson, N. Hance, K. Naess, K. Tear-Fahnehjelm, U. von Dobeln, K. Majamaa, N.G. Larsson, Secondary metabolic effects in complex I deficiency, Ann. Neurol. 58 (2005) 544–552.
[65] P. Risiglione, L. Leggio, S.A.M. Cubisino, S. Reina, G. Paterno, B. Marchetti, A. Magri, N. Iraci, A. Messina, High-resolution respirometry reveals MPP(+) mitochondrial toxicity mechanism in a cellular model of Parkinson's disease, Int. J. Mol. Sci. 21 (2020).
[66] A.J. Worth, S.S. Basu, N.W. Snyder, C. Mesaros, I.A. Blair, Inhibition of neuronal cell mitochondrial complex I with rotenone increases lipid beta-oxidation, supporting acetyl-coenzyme a levels, J. Biol. Chem. 289 (2014) 26895–26903.
[67] H.E. Thomas, Y. Zhang, J.A. Stefely, S.R. Veiga, G. Thomas, S.C. Kozma, C. A. Mercer, Mitochondrial complex I activity is required for maximal autophagy, Cell Rep. 24 (2018) 2404–2417 e2408.
[68] L. Robke, Y. Futamura, G. Konstantinidis, J. Wilke, H. Aono, Z. Mahmoud, N. Watanabe, Y.W. Wu, H. Osada, L. Laraia, H. Waldmann, Discovery of the novel autophagy inhibitor aumitin that targets mitochondrial complex I, Chem. Sci. 9 (2018) 3014–3022.
[69] K. Kagedal, W.S. Kim, H. Appelqvist, S. Chan, D. Cheng, L. Agholme, K. Barnham, H. McCann, G. Halliday, B. Garner, Increased expression of the lysosomal cholesterol transporter NPC1 in Alzheimer's disease, Biochim. Biophys. Acta 2010 (1801) 831–838.